© 2020. Published by The Company of Biologists Ltd | Development (2020) 147, dev182469. doi:10.1242/dev.182469

RESEARCH ARTICLE

Cilia-driven asymmetric Hedgehog signalling determines the amphioxus left-right axis by controlling *Dand5* expression

Xin Zhu, Chenggang Shi, Yanhong Zhong, Xian Liu, Qiuning Yan, Xiaotong Wu, Yiquan Wang* and Guang Li*

ABSTRACT

Cilia rotation-driven nodal flow is crucial for the left-right (L-R) break in symmetry in most vertebrates. However, the mechanism by which the flow signal is translated to asymmetric gene expression has been insufficiently addressed. Here, we show that Hedgehog (Hh) signalling is asymmetrically activated (L<R) in the region in which initial asymmetric *Dand5* expression is detected. Upregulation of Hh signalling on the left side of wild-type embryos induces ectopic *Dand5* expression on the left side, and the unilateral recovery of Hh signalling in *Hh* homozygous mutants induces *Dand5* expression in the Hh signal recovery side. Immunofluorescence analysis results revealed that Hh fusion protein is asymmetrically enriched in the anterior-right paraxial mesoderm at the early neurula stage. Inhibiting embryonic cilia motility using methylcellulose (MC) blocks Hh protein enrichment on the right hand side and randomizes *Dand5* expression and organ positioning along the L-R axis. These findings present a model showing that cilia movement is crucial for the symmetry breaks in amphioxus through asymmetric Hh protein transport. The resultant asymmetric Hh signalling provides a clue into the induction of asymmetric *Dand5* expression.

This article has an associated 'The people behind the papers' interview.

KEY WORDS: Amphioxus, Left-right asymmetry, Embryonic development, Hh signalling, Cilium

INTRODUCTION

Bilateral symmetry is a fundamental feature of many animal phyla that are generally called bilateria. Most bilateria deviate from bilateral symmetry in a predictable manner known as directional left-right (L-R) asymmetry (Palmer, 1996). The establishment of L-R asymmetry during early embryogenesis is crucial for the correct positioning and morphogenesis of internal organs (Sutherland and Ware, 2009). The mechanism that initiates L-R asymmetric organogenesis is one of the central enigmas in developmental biology. In vertebrates, L-R asymmetry originates at a transient midline structure known as the L-R organizer (LRO), which forms at the posterior end of the notochord during the early somite stages (Blum et al., 2009, 2014). Each LRO cell harbours a motile monocilium that rotates clockwise to generate a leftward fluid flow (nodal flow) that acts as the breaking mechanism of L-R symmetry in mouse, *Xenopus* and zebrafish (Nonaka et al., 1998; Schweickert et al., 2007; Essner et al., 2005). Recent studies have also shown a role for motile cilia in the L-R asymmetric establishment of urochordate and sea urchin embryos (Nishide et al., 2012; Tisler et al., 2016). This result thus indicates that cilia-based symmetry breaking is a synapomorphy of the deuterostome. However, whether any invertebrate deuterostome harbours a homologue of the LRO remains to be investigated.

In most vertebrate embryos, nodal flow is an initial driving force for symmetry breaking, and several genes involved in L-R asymmetry development are expressed asymmetrically as a result of the flow (Okada et al., 2005; Blum et al., 2009). Among these genes, *Dand5* (also known as *Cerberus*; *Cerl2* in mouse, *Charon* in zebrafish and *Coco* in frog) first shows asymmetric expression around the LRO in an R>L manner (Schweickert et al., 2010; Nakamura et al., 2012). As Dand5 is a repressor of Nodal, Nodal near the LRO is next to show L>R asymmetry, which in turn induces an asymmetric signalling cascade in the left lateral plate mesoderm, directing the embryo to develop an L-R asymmetric pattern (Schweickert et al., 2010; Grimes and Burdine, 2017; Hashimoto et al., 2004). Although the role of nodal flow in L-R symmetry breaking in vertebrates has been addressed, how nodal flow is sensed and transduced into asymmetric gene expression remains unknown.

To date, two models, the two-cilia model and the morphogen model, have been proposed to explain the mechanism by which nodal flow breaks L-R symmetry. The two-cilia model posits that there are two classes of cilia on the LRO: one is composed of motile cilia located at the centre of the LRO and essential for generating the leftward flow, and the other comprises immotile cilia, present at the periphery of the LRO and crucial for sensing the flow (McGrath et al., 2003; Tabin and Vogan, 2003). The two-cilia model is also based on the proposition that the shear stress generated by the flow is different on the left side than it is on the right side of the LRO, and such a difference, after being sensed by the immotile cilia, results in the elevation of the calcium signal and asymmetric expression of the *Nodal* gene on the left side (McGrath et al., 2003; Tabin and Vogan, 2003). This model explains many phenomena found in vertebrates with mutant cilia and L-R defects, but it has recently been challenged by both *in vitro* experiments and *in silico* simulations (Delling et al., 2016; Ferreira et al., 2017). The morphogen model posits that the nodal flow is crucial for transporting the morphogen 'X' to the left side of the LRO, where the 'X' is sensed by receptors in the cells or cilia, resulting in asymmetric gene expression (Tanaka et al., 2005; Tabin and Vogan, 2003). Nodal vesicular parcels (NVPs) that carry Sonic hedgehog (Shh) and retinoic acid (RA) have been found to be transported preferentially to the left side of the mouse LRO by the flow (Tanaka et al., 2005). However, no obvious asymmetry of Shh or retinoid signalling has been detected at the mouse LRO (Tabin, 2006), and knocking out the *Shh* or *Raldh2* (a gene involved in RA synthesis; also known as *Aldh1a2*)

State Key Laboratory of Cellular Stress Biology, School of Life Sciences, Xiamen University, Xiamen, Fujian 361102, China.

*Authors for correspondence (guangli@xmu.edu.cn; wangyq@xmu.edu.cn)

X.Z., 0000-0002-9712-0089; C.S., 0000-0002-5592-2761; Y.Z., 0000-0002-6142-0362; X.L., 0000-0001-8509-6926; Q.Y., 0000-0002-3644-9876; X.W., 0000-0003-2959-5602; Y.W., 0000-0002-3305-7535; G.L., 0000-0002-5543-5349

Received 10 July 2019; Accepted 27 November 2019

Development (2020) 147, dev182469. doi:10.1242/dev.182469

genes in mice caused no effects on the initial L-R determination (Tsukui et al., 1999). To date, the asymmetric distribution of Shh or RA has not been reported for LROs in other vertebrate species. Therefore, to determine whether Shh or RA has a role as the morphogen 'X', further investigation is required.

Among living invertebrate deuterostomes, amphioxus is of particular importance in studying the molecular mechanisms of vertebrate embryogenesis owing to its basal position within the phylum Chordata and its simple, but vertebrate-like, genome structure, embryogenesis and body plan (Holland et al., 2004; Putnam et al., 2008). In terms of L-R asymmetry, amphioxus shows pronounced L-R morphology at the larval stage, with the mouth and pre-oral pit forming on the left side, gill slits and a major part of the endostyle and club-shaped gland presenting on the right side (Soukup, 2017). Moreover, in contrast to the sophisticated phenotypes found in vertebrates, knocked out (or knocked down) or mis-expressed *Dand5*, *Nodal* and/or *Lefty* genes in amphioxus usually results in two kinds of bilateral defects: two-left (left-isomerism) and two-right (right-isomerism) phenotypes (Li et al., 2017; Soukup, 2017). Importantly, amphioxus also utilizes a signalling cascade composed of Dand5, Nodal, Lefty and Pitx in the patterning of the L-R asymmetry (Li et al., 2017). These features and their outcomes indicate that amphioxus is a useful and informative model for investigating the origin and mechanism of nodal flow. Interestingly, we recently found that *Dand5* transcription in amphioxus embryos relies on the *Hedgehog* (*Hh*) gene (Hu et al., 2017). This finding indicates a potential role for Hh in the regulation of the asymmetric expression of *Dand5* in amphioxus. In this report, we first investigate whether Hh signalling in amphioxus is asymmetrically activated using *in situ* hybridization and then clarify the role of Hh signalling in the regulation of asymmetric *Dand5* expression. Furthermore, we investigate the role of cilia in asymmetric Hh signalling formation and initial symmetry breaking by disrupting the function of the cilia through genetic manipulation, brief high-salt treatments and a MC treatment. Together, the findings identify cilia movement and asymmetric Hh signalling as the two key regulators for the establishment of amphioxus L-R asymmetry, and we used this conclusion to propose a novel mechanism for L-R symmetry breaking in amphioxus.

RESULTS

Hh signalling activity in early amphioxus neurulae

Our recent results have shown that Hh signalling is required for *Dand5* transcription in amphioxus (Hu et al., 2017). However, whether Hh signalling is asymmetric in developing embryos and whether this possible asymmetry is the cause of asymmetric *Dand5* expression remain unknown. Hh (ligand), Ptch (receptor), Smo (signal transducer) and Gli (transcription factor) are the key components of the Hh signalling pathway. To address the questions raised, we previously analyzed *Hh* and *Ptch* gene expression during several stages of amphioxus embryos with the whole-mount *in situ* hybridization (WISH) method and detected no obvious asymmetric expression signal for either of these two genes (Hu et al., 2017). In the present study, we reanalyzed the expression pattern of these two genes and extended the analysis to the *Smo* and *Gli* genes. Specifically, to observe the staining signal more clearly, we conducted serial transverse section analysis on embryos after the WISH analysis was completed. Four sequential stages of embryos after the G5 stage (in the late gastrula stage, according to Hirakow and Kajita, 1991) were analyzed, with the observation continuing for an additional 90 min (until approximately the N1 stage, according to Hirakow and Kajita, 1994), during which time, the symmetric *Dand5* expression was converted to show asymmetric expression (Fig. 1Aa-Ad). The results showed that in both the whole embryos (Fig. 1Ba-Dd) and in the transverse sections (Fig. 1Bc′-Dc′), *Hh* was symmetrically expressed in the axial mesoderm and gut endoderm, and *Smo* and *Gli* were symmetrically expressed in the paraxial mesoderm. However, in the anterior paraxial mesoderm of some examined embryos, very weak asymmetric expression (L<R) was detected for the *Ptch* gene (Fig. 1Ea-Ed). Transverse sections confirmed this observation (Fig. 1Ea′-Ed′). At the G5 stage, among the fourteen examined embryos, six (42.8%) showed L<R *Ptch* expression in the anterior mesoderm (Fig. 1Ea′), and at the subsequent three examined stages, the percentage of the embryos showing asymmetric *Ptch* expression increased to 73.9% (17/23), 90.9% (20/22) and 100% (16/16), respectively (Fig. 1Eb′-Ed′) (Fig. S1). As *Ptch* and *Gli* are targets of the Hh signalling pathway in vertebrates (Hooper and Scott, 2005; Lee et al., 1997), we analyzed the expression of *Ptch* and *Gli* in $Hh^{-/-}$ embryos at the early neurula stage of amphioxus to determine whether they are also regulated by Hh signalling. Compared with that of the $WT/Hh^{+/-}$ embryos, *Ptch* expression was dramatically decreased in the $Hh^{-/-}$ embryos, but the *Gli* expression was not obviously affected (Fig. S2). This result indicates that *Ptch* is regulated by Hh signalling, whereas *Gli* is not, at least not at this stage of amphioxus embryonic development. From this, and the observed asymmetric expression of the *Ptch* gene, we suggest that Hh signalling is asymmetric in the early neurula stage of amphioxus embryos. Importantly, we also observed that the initial time and the region of asymmetric *Ptch* expression resembled those of the *Dand5* gene (Fig. 1Aa-Ad,Ac′,Ea′-Ed′,F). This observation, together with previous findings (Hu et al., 2017), indicates that asymmetric Hh signalling might provide an initial cue for asymmetric *Dand5* expression.

Ectopic *Dand5* expression induced by the upregulation of Hh signalling

To further address the relationship between Hh signalling and *Dand5* expression, we examined whether increasing Hh signalling activity could induce the ectopic expression of *Dand5*. *Ptch* is a target and negative regulator of Hh signalling in vertebrates and flies. We anticipated that, if this were the same case in amphioxus, mutation of the *Ptch* gene in amphioxus would result in upregulation of Hh signalling and *Ptch* expression. To test this hypothesis, we examined *Ptch* expression in *Ptch* mutant embryos at the N1 stage (approximately three somites at this stage). Unexpectedly, we found no obvious difference in *Ptch* expression between the $Ptch^{-/-}$ embryos and their siblings (Fig. S3). Moreover, we found that injection of *Hh* mRNA into the *Ptch* mutants led to the upregulation of *Ptch* expression (Fig. S3). These results indicate that the *Ptch* mutant might not be a null mutant or that Hh may transduce Hh signalling via other receptors in amphioxus. Consistent with this speculation, the $Ptch^{-/-}$ mutants expressed the *Dand5* gene normally (L<R) at the N1 stage and exhibited no L-R defects at the larval stage (Hu et al., 2017).

We then injected amphioxus embryos with mRNAs coding the Hh protein or a constitutively active form of the Smo protein (caSmo) to increase Hh signalling. We found that both injections could effectively upregulate Hh signalling, as indicated by increased *Ptch* expression (Fig. S4). The injection of *caSmo* mRNA also changed the *Dand5* expression pattern. In the uninjected control embryos, *Dand5* was expressed predominantly on the right side (right side-specific or L<R) (Fig. 2A,B), whereas in the *caSmo* mRNA-injected embryos, 41.7% (10/24) showed bilaterally symmetric *Dand5* expression (Fig. 2E) and 4.2% (1/24) displayed

Development (2020) 147, dev182469. doi:10.1242/dev.182469

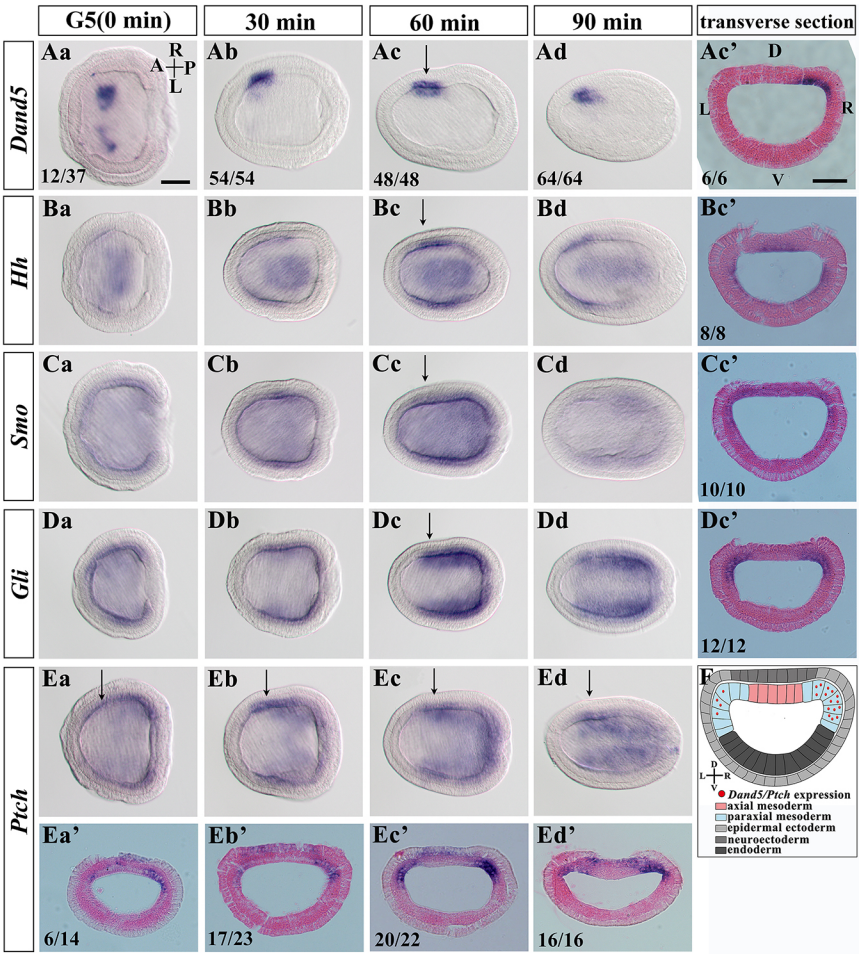

Fig. 1. The expression of *Dand5*, *Hh*, *Smo*, *Gli* and *Ptch* genes in developing amphioxus embryos. (Aa-Ad) Representative examples of *Dand5* expression patterns during the four development stages. Arrow in Ac marks the section plane in Ac′. (Ac′) Transverse section shows *Dand5* asymmetric expression in the right axial mesoderm. (Ba-Bd) Representative examples of the *Hh* expression pattern during the four development stages. Arrow in Bc marks the section plane in Bc′. (Bc′) Transverse section of an embryo showing *Hh* symmetric expression in the axial mesoderm and gut endoderm. (Ca-Dd) Representative examples of *Smo* and *Gli* expression patterns at the four development stages. The arrow in Cc and Dc mark the section plane in Cc′ and Dc′, respectively. (Cc′ and Dc′) Transverse section shows *Smo* and *Gli* symmetric expression in the left and right axial mesoderm. (Ea-Ed) Representative examples of *Ptch* expression patterns at the four development stages. The arrows in Ea-Ed mark the section plane in Ea1′-Ed′, respectively. (Ea′-Ed′) Transverse sections show asymmetric *Ptch* expression (R>L) in the anterior paraxial mesoderm. (F) Schematic of the cross-section of an early neural amphioxus embryo. Images in panels A-E were taken from the dorsal view with the anterior to the left. Time at the G5 stage is defined as 0 min, and the data from the subsequent three stages were analyzed. Numbers in the bottom left corner of some panels show the number of times asymmetric expression was observed in the total number of embryos examined; the remainder of the embryos did not show asymmetric gene expression. A, anterior; D, dorsal; L, left side; P, posterior; R, right side; V, ventral. Scale bar: 50 µm in Aa (for A-E) and Ac′ (for A′-E′).

reversed *Dand5* expression (L>R) (Fig. 2F), although the remaining 54.1% (13/24) expressed *Dand5* normally in a L<R manner (Fig. 2C,D). Consistent with these findings, 20% (10/50) of the *caSmo* mRNA-injected embryos presented with the right-isomerism phenotype (Fig. 3C-E) at the larval stage. This phenotype was not presented by the uninjected control embryos (Fig. 3A,B,E). We also injected *caSmo* mRNA into the right- and left-side blastomere immediately after the first cleavage, as shown in Fig. 2O. The results showed that the right-side injection had no effect on the *Dand5* expression pattern (R>L, similar to that of the uninjected control embryos) (Fig. 2G-J), but the left-side injection caused L=R and L>R *Dand5* expression in 22% (8/36) and 5.5% (2/36) of the embryos, respectively (Fig. 2M,N), although the remaining embryos expressed the gene normally in a right side-specific or L<R manner (Fig. 2K,L). Combined, these data demonstrate that upregulating Hh signalling on the left side could induce ectopic *Dand5* expression.

Side-specific *Dand5* expression in $Hh^{-/-}$ embryos through the unilateral recovery of Hh signalling

To determine whether asymmetric Hh signalling is the cause of asymmetric *Dand5* expression, we recovered Hh signalling in one side of the $Hh^{-/-}$ mutants by injecting *caSmo* mRNA at the two-cell stage and then examined the *Dand5* expression at the early neurula stage. No *Dand5* expression signal appeared in the $Hh^{-/-}$ embryos (15/15) (Fig. 3G). However, *caSmo* mRNA injection on the right side of the $Hh^{-/-}$ mutant led to 87.5% (7/8) embryos with right side-specific *Dand5* expression (Fig. 3H). Remarkably, among the $Hh^{-/-}$ embryos injected on the left side, 70% (7/10) showed *Dand5* expression on the left side only (Fig. 3I). We verified this result by injecting *Hh* mRNA into the right and left sides of the $Hh^{-/-}$ mutant embryos. The results showed that 80% (4/5) of right-side injected $Hh^{-/-}$ embryos expressed *Dand5* on the right and 75% (6/8) of left-side injected embryos expressed *Dand5* on the left (Fig. 3K,L), whereas none of the nine uninjected $Hh^{-/-}$ embryos showed *Dand5* expression (Fig. 3J). Together with the data described above, the results indicate that asymmetric Hh signalling directs asymmetric *Dand5* expression in amphioxus.

Asymmetric enrichment of the Hh protein in the anterior-right paraxial mesoderm of early neurulae

We demonstrated above that the left-side injection of *Hh* mRNA could induce *Dand5* expression on the left side in the $Hh^{-/-}$ embryos. However, when we injected *Hh* mRNA into the $Hh^{-/-}$ embryos at the one-cell stage, most showed an L<R *Dand5* expression pattern but not a bilaterally symmetric pattern (Fig. S5). Moreover, a higher proportion of wild-type embryos injected with *caSmo* mRNA at the unfertilized egg stage had the right-isomerism phenotype (10/50=20%) than the proportion of offspring of the $Hh^{+/-}$ heterozygotes injected with *Hh* mRNA at the unfertilized egg stage (6/62=9.7%; Fig. 3E,F). We speculated that the discrepancy between the results of the *caSmo* and *Hh* mRNA injections might be caused by an asymmetric transport of the Hh protein to the right side. Because no commercial antibody against amphioxus Hh protein is available, we injected amphioxus unfertilized eggs with mRNA coding a Myc-tagged Hh protein and examined the Hh

Development (2020) 147, dev182469. doi:10.1242/dev.182469

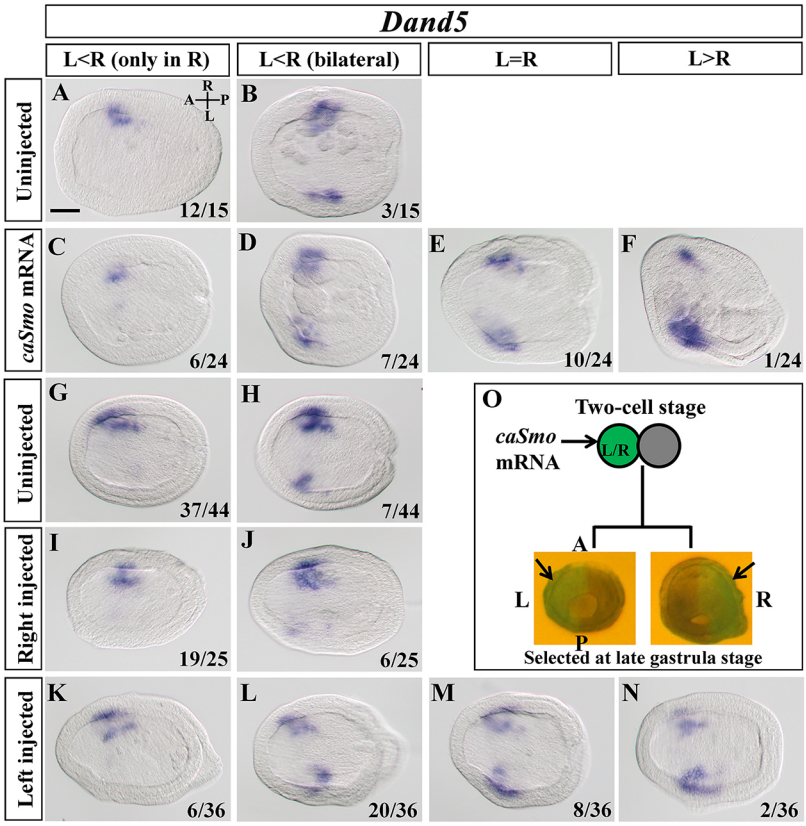

Fig. 2. Overactivation of Hh signalling induces ectopic *Dand5* expression on the left side of the embryos in the early neurula stage. (A-F) Expression patterns of *Dand5* in uninjected embryos (A,B) and *caSmo* mRNA-injected embryos (C-F) at the early neurula stage. (G-N) Expression patterns of *Dand5* in uninjected embryos (G,H) and *caSmo* mRNA injected into right side (I,J) or left side (K-N) of the embryos at the early neurula stage. (O) Schematic of the right side and the left side injection spots. Images are taken from the dorsal view of the anterior to inside. mRNA was injected randomly into one blastomere of WT embryos at the two-cell stage. They were separated into left-side injected and right-side injected embryos under a fluoroscope at the G5 stage. Arrows pointing to green fluorescence indicate the side injected. Images in panels A-N were taken from the dorsal view with the anterior to the left. Numbers in the bottom right corner of a panel show the number of times the phenotype was observed in the total number of embryos examined. A, anterior; D, dorsal; L, left side; P, posterior; R, right side; V, ventral. Scale bar: 50 µm in A (for A-N).

fusion protein distribution using whole-mount immunofluorescence (WIF) with a Myc antibody. The injection rescued *Dand5* expression and the L-R morphology of the $Hh^{-/-}$ embryos (Fig. S6), suggesting that the Hh-Myc fusion protein works as an endogenous Hh protein. Theoretically, the fused protein would be detected widely throughout the injected embryos. However, in contrast to this expectation, we observed an asymmetric staining signal (L<R) in the anterior paraxial mesoderm in 40% (2/5) of G5-stage gastrulae, in 100% (6/6) of the R0 neurulae (final gastrulae or early neurulae at stage G7 according to Hirakow and Kajita, 1991; embryos start rotating at this stage) and in 75% (6/8) of the R30 neurulae (30 min after initial rotation, at approximately the N1 neurula stage) (Fig. 4D-F″). This pattern is reminiscent of the endogenous expression pattern of *Ptch* and *Dand5* mRNA (Fig. 1). No staining signal was detected in the uninjected embryos (Fig. 4A-C). Further immunoelectron microscopy analysis revealed that the Hh-Myc protein was localized in the extracellular interface of the ectoderm and paraxial mesoderm (Fig. S7). These results suggest that the asymmetric distribution of the Hh protein is likely the cause of the asymmetric Hh signalling demonstrated above.

Cilia and L-R asymmetry in amphioxus embryos

The L-R asymmetric distribution of the Hh protein in amphioxus embryos raises the issue of whether the amphioxus embryo has a nodal flow similar to that in vertebrates. To address whether cilia are required for L-R asymmetric development in amphioxus, we generated mutants of the *Kif3a* or *Foxj1* genes, which are required for ciliogenesis in vertebrates (Marszalek et al., 1999; Tamakoshi et al., 2006; Yu et al., 2008), using the TALEN method.

The *Kif3a* mutants had a 20 bp deletion of ∼110 bp downstream of the start codon (Fig. S8A). At the larval stage, compared with their heterozygous ($Kif3a^{+/-20}$) and wild-type siblings (Fig. S8B,D,D′), the $Kif3a^{-20/-20}$ mutants developed an enlarged mouth and fewer cilia in the pre-oral pit, but they presented with normal L-R asymmetry (Fig. S8C,E,E′). A comparison between $Kif3a^{-20/-20}$ and wild-type ($Kif3a^{+/+}$) early neurulae did not reveal any obvious differences in either the pattern or the length of the cilia on the epithelial ectodermal (EE) cells, neural ectodermal (NE) cells or the gastrocoel roof plate (GRP) cells (Fig. S8G-J,K). The inability of the *Kif3a* mutation to effect early ciliogenesis is likely caused by its strong maternal expression (Fig. S8L). Two mutant lines in the *Foxj1* coding region were generated: one with a 1 bp deletion at position +318 bp and one with a 13 bp deletion at the beginning of the forkhead domain (Fig. S9A,B). However, neither of these mutants showed abnormalities in ciliogenesis or the L-R asymmetric axis. The cilia lengths on the EE, NE or GRP cells at the early neurula stage were similar to those of their wild-type siblings (Fig. S9C-F). The cilia movement in the $Foxj1^{-1/-1}$ mutants had no apparent defect (Movie 1). The transcriptome data for different developmental stages (Fig. S9H) and the *in situ* hybridization (Aldea et al., 2015) revealed negligible *Foxj1* mRNA expression in the fertilized eggs and embryos until the gastrula stage, indicating that the inability of *Foxj1* to disrupt ciliogenesis is not due to maternal expression.

To remove the amphioxus embryo cilia, we then tried a physical method in which we treated the embryos with high-salt (HS) seawater, a method that had been applied to sea urchin embryos (Auclair and Siegel, 1966; Tisler et al., 2016). The treatment removed most cilia from the embryos, as indicated by the evidence from the immunofluorescence analysis in which an antibody against acetylated-α-tubulin was used (Fig. S10A-D). After the treatment, the expressions of *Brachyury* (a marker of posterior mesoderm and of the presumptive notochord; Holland et al., 1995) and *Netrin* (a marker of the floorplate of the presumptive neural tube and the notochord;

Development (2020) 147, dev182469. doi:10.1242/dev.182469

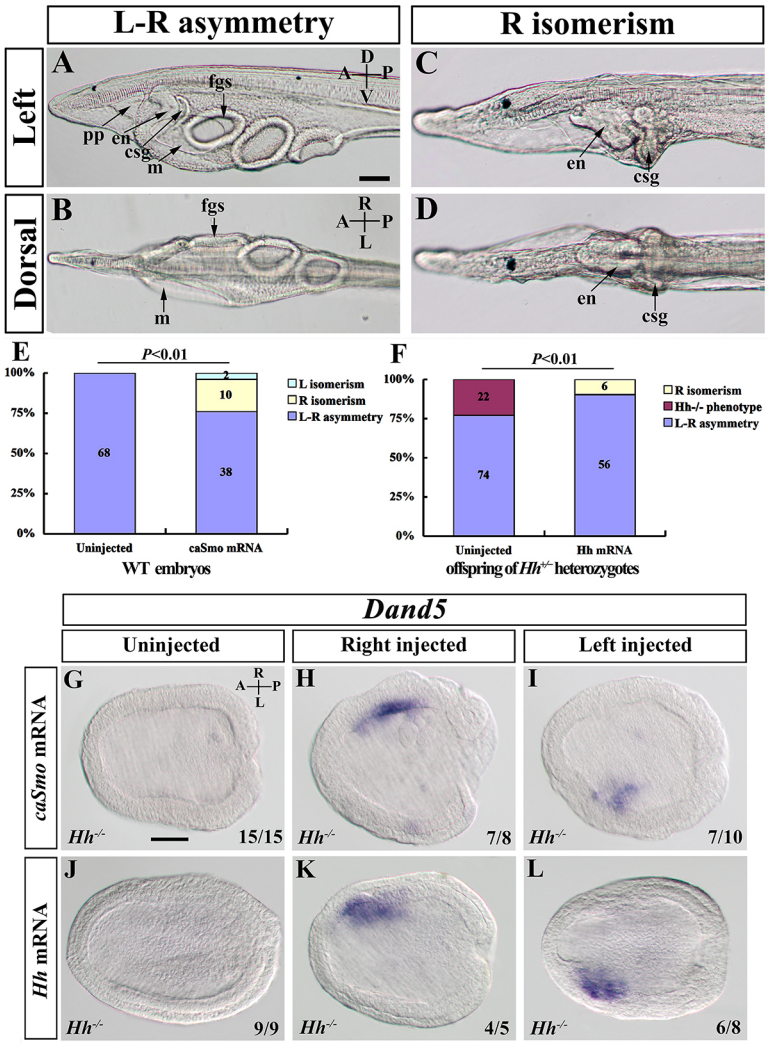

Fig. 3. Overactivation of Hh signalling causes the right-isomerism phenotype, and unilateral activation of Hh signalling induces *Dand5* expression on the activated side of the *Hh*$^{-/-}$ embryos. (A,B) Asymmetric morphology of the control larvae. A shows a left lateral view of the pharyngeal region with focus on the right side, showing the left-side pre-oral pit (pp), right-side endostyle (en) and club-shaped gland (csg). B shows a dorsal view of the pharyngeal region focused on the ventral side. fgs, first gill slit; m, mouth. (C,D) Overactivation of Hh signalling causes right-isomerism morphologies. C shows a left lateral view of the pharyngeal region focused on the sagittal plane, showing the improperly developed en and csg. No mouth opening or pp were observed. D shows a dorsal view of the pharyngeal region focused on the ventral side, showing the morphological symmetry of en and csg resulting from the duplication of the right-side parts of en and csg. (E,F) Quantification of embryos showing normal (L-R asymmetry), right-isomerism, left-isomerism and *Hh*$^{-/-}$ mutant phenotypes. (G-I) Expression patterns of *Dand5* in uninjected and *caSmo* mRNA-injected *Hh*$^{-/-}$ embryos at the early neurula stage. (J-L) Expression patterns of *Dand5* in the uninjected and *Hh* mRNA-injected *Hh*$^{-/-}$ embryos at the early neurula stage. Images in G-L were taken from the dorsal side with the anterior to the left. Numbers in the bottom right corner of a panel show the number of times the phenotype was observed in the total number of embryos examined. A, anterior; D, dorsal; L, left side; P, posterior; R, right side; V, ventral. Scale bar: 50 µm in A (for A-D) and G (for G-L).

Shimeld, 2000) were unaffected compared with the untreated control embryos (Fig. S11A-D′). This finding indicates that the midline structures (including the neural plate and notochord) were formed normally in the treated embryos. However, the treatment caused 54.5% (12/22) of the embryos to lose *Dand5* expression (Fig. 5C-E), and 78.1% (25/32) and 53.8% (28/52) of the embryos, respectively, to express *Nodal* and *Pitx* bilaterally (Fig. 5F-K). In agreement with this finding, 48.6% (17/35) of the treated embryos displayed a left-isomerism phenotype at the larval stage (Fig. 5A-B′). This observation demonstrates that cilia are required for the establishment of L-R asymmetry in amphioxus.

Involvement of cilia movement, but not embryo rotation, in the L-R asymmetry development of amphioxus

MC is a nontoxic viscous reagent used for inhibiting LRO cilia movement in vertebrates (Schweickert et al., 2007; Shinohara et al., 2012). To clarify the role of cilia movement without disrupting ciliogenesis, we blocked cilia movement by culturing embryos from the mid-gastrula to the R30 or three-somite stage in seawater containing 2% MC. The MC could enter the archenteron through the blastopore, as indicated by the presence of ink particles (added to the MC) in the archenteron of the three-somite embryos (Fig. 6A), and effectively inhibit cilia movement and neurula rotation (Movie 2), but no apparent effect on the expression of *Brachyury* or *Netrin* was found at the early neurula stage (Fig. S11E-H′). At the larval stage, 56.6% (48/85) of the treated larvae displayed L-R asymmetry defects (Fig. 6B). Among them, 83.3% (40/48) showed a left-isomerism phenotype, 12.5% (6/48) showed a right-isomerism phenotype, and the remaining 4.2% (2/48) exhibited an L-R reversal phenotype (Fig. 6B). *Dand5* expression along the L-R axis was randomized by the treatment, with 44% (11/25) presenting as normal (L<R), 24% (6/25) being absent, 24% (6/26) presenting a bilateral phenotype (L=R), and 8% (2/25) showing reversed phenotype (L>R) (Fig. 6C-G). The expression levels of *Nodal* and *Pitx* were also altered in 65.5% (19/29) and 67.7% (21/31) of the treated embryos, respectively, and were either expressed bilaterally (L=R), were not expressed (or had decreased expression) or were expressed in the reverse pattern (L<R) (Fig. 6H-Q). We also analyzed the effect of MC treatment on *Ptch* expression to determine whether asymmetry of Hh signalling was affected. In the control embryos, *Ptch* is asymmetrically expressed in an L<R pattern in the paraxial mesoderm of the early neurulae (7/7; Fig. 6R). However, after MC treatment, 42.9% (6/14) and 14.2% (2/14) of the early neurulae showed bilateral (but decreased) and L>R *Ptch* expression in the paraxial mesoderm, respectively (Fig. 6T,U), although the remaining 42.9% (6/14) of them displayed a normal L<R *Ptch* expression (Fig. 6S). These results indicate that cilia movement is necessary for the establishment of asymmetric Hh signalling and L-R asymmetry development in amphioxus.

Development (2020) 147, dev182469. doi:10.1242/dev.182469

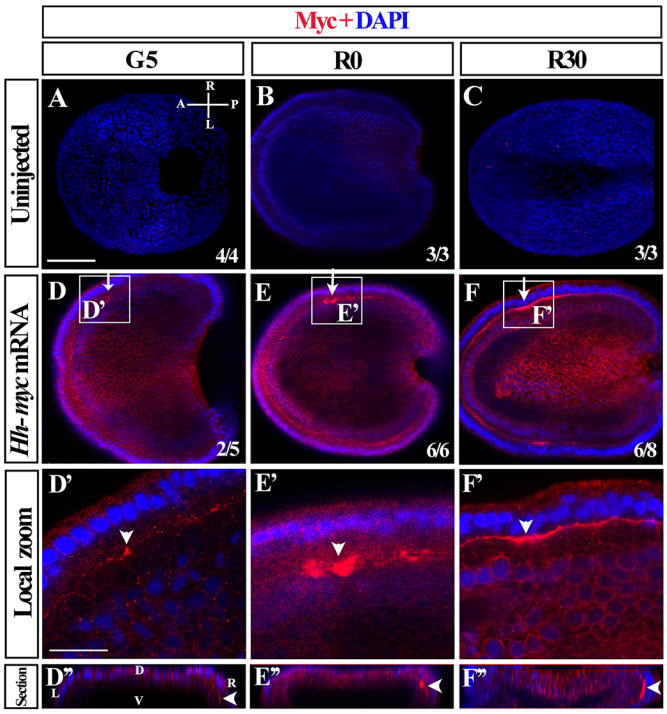

Fig. 4. Asymmetric enrichment of the Hh protein in the anterior right paraxial mesoderm of early neurulae. (A-F) Immunofluorescence images of uninjected and *Hh-myc* mRNA-injected embryos at the G5, R0 (beginning to rotate) and R30 (30 min after R0) neurula stages. Hh-Myc fusion protein is labelled with the Myc antibody (red), and the cell nuclei are labelled with DAPI (blue). There is no Myc signal in the uninjected embryos (A-C), whereas the Hh-Myc fusion protein is asymmetrically enriched in the anterior right paraxial mesoderm of the G5, R0 and R30 stage embryos (D-F). D′-F′ show a magnification of the white boxed area of panels D-F, respectively. D″-F″ show section planes at levels indicated in D-F (arrows). Arrowheads in D′-F′ and D″-F″ point to asymmetric enrichment of Hh fusion protein in the right paraxial mesoderm. Images in A-F were taken from the dorsal view with the anterior to the left. Numbers in the bottom right corner of a panel show the number of times the phenotype was observed in the total number of embryos examined. A, anterior; D, dorsal; L, left side; P, posterior; R, right side; V, ventral. Scale bar: 50 µm in A (for A-F); 20 µm in D′ (for D′-F′).

Neurula rotation driven by motile cilia is required for the L-R patterning in the ascidian *Halocynthia roretzi* (Nishide et al., 2012). To verify that the L-R defect induced by the MC treatment was caused by the inhibited cilia movement, but not the neurula rotation, we fixed the embryos at the G4 stage (later mid-gastrula stage) by threading them through a very fine glass needle (Fig. S12A,B) and released them at the three-somite stage. Ninety-nine embryos were analyzed, and six of them showed L-R defects at the larval stage (five larvae developed a left-isomerism phenotype, and one exhibited a right-isomerism phenotype) (Fig. S12C). This finding was not significantly different from that of the control (P=0.1431, Fisher exact test), in which two of the 124 embryos examined showed a left-isomerism phenotype (Fig. S12C). This result indicates that cilia movement, but not embryo rotation, is essential for the L-R asymmetric development in amphioxus.

Cilia movement and asymmetric transport of the Hh protein

In mice, NVPs containing the Shh protein can be asymmetrically transported across the node by the cilia-driven flow (Tanaka et al., 2005). To determine whether cilia movement is also involved in the asymmetric distribution of the Hh protein in amphioxus, we injected the embryos with *Hh-myc* mRNA and then cultured them with 2% MC as described above. Immunofluorescence analysis showed that 70% (7/10) of the injected embryos cultured in regular seawater had right-side enrichment of the Hh-Myc protein in the anterior-right paraxial mesoderm (Fig. 7A-B″). However, all (11/11) of the embryos injected with the *Hh-myc* mRNA and cultured in 2% MC failed to accumulate the secreted Hh-Myc protein in the right paraxial mesoderm (Fig. 7C-D″). In addition, the *Hh* mRNA-injected embryos cultured in 2% MC had a higher frequency of bilateral *Dand5* expression than those cultured in regular seawater (Fig. S13). These results indicate that cilia movement plays an essential role in the asymmetric transportation of the Hh protein.

Requirement of cilia in the transduction of Hh signalling in amphioxus

HS seawater-treated embryos showed similar phenotypes (lost *Dand5* expression and bilateral *Nodal* expression; Hu et al., 2017) to those acquired by the *Hh*-knockout embryos. Indeed, *Ptch* expression was significantly downregulated in the HS-treated amphioxus embryos at the early neurula stage (Fig. S10E-G). These findings raise the possibility that the L-R defect induced by the HS treatment might be a secondary effect of impaired Hh signal transduction. To address this possibility, we investigated whether Hh signal transduction relies on cilia in amphioxus in a manner similar to the signal transduction in sea urchins and vertebrates. In vertebrates, the translocation of the Smo protein from the cytoplasm to the cilium serves as a marker for Hh signal activation (Huangfu et al., 2003; Warner et al., 2014), which is initiated through a ciliary localization motif in the Smo protein. We identified a similar ciliary localization motif in the amphioxus Smo protein. The results from the immunofluorescence analysis on the embryos injected with mRNA encoding caSmo-Myc and CLDcaSmo-Myc (carrying mutations in the ciliary localization motif) showed that, although the caSmo-Myc fusion protein was conspicuously detected on the cilia on the neuroectodermal and paraxial mesoderm cells (Fig. 8B-B″ and Fig. S14C,D) where endogenous *Ptch* expression was also detected (Fig. 1Ea′-Ed′), CLDcaSmo-Myc failed to locate to any cilia (Fig. 8C-C″). No Smo-Myc protein (red signal) was observed in the uninjected embryos (Fig. 8A-A″). Furthermore, *Ptch* expression was significantly increased in the *caSmo-myc* mRNA-injected embryos but not in the *CLDcaSmo-myc* mRNA-injected embryos, with respect to the levels expressed by the uninjected embryos (Fig. 8D-G). These results suggest that Hh signal transduction in amphioxus relies on cilia, and the abnormal phenotypes of L-R asymmetry caused by removing cilia in the HS treatment might be the result of a dysfunction in Hh signalling.

DISCUSSION

L-R asymmetry formation in vertebrates involves three major steps: symmetry breaking by cilia-driven nodal flow, asymmetric activation of gene expression and asymmetric organogenesis. Using the TALEN-based genome editing and heat shock promoter-driven overexpression method, we recently demonstrated that asymmetric genes, such as *Dand5*, *Nodal*, *Lefty* and *Pitx*, are also required for amphioxus L-R development, similar to their cognates in vertebrates (Li et al., 2017). In addition, we also found that the Hh gene is required for *Dand5* expression in amphioxus (Hu et al., 2017). In this study, we identified cilia movement and asymmetric Hh signalling as two key regulators for the establishment of amphioxus L-R asymmetry. Based on these findings, we constructed a comprehensive model (Fig. 9) to explain how amphioxus L-R asymmetry is initially established. Our model suggests that, at late gastrula (G5) and early neurula (N1) stages, cilia movement

Development (2020) 147, dev182469. doi:10.1242/dev.182469

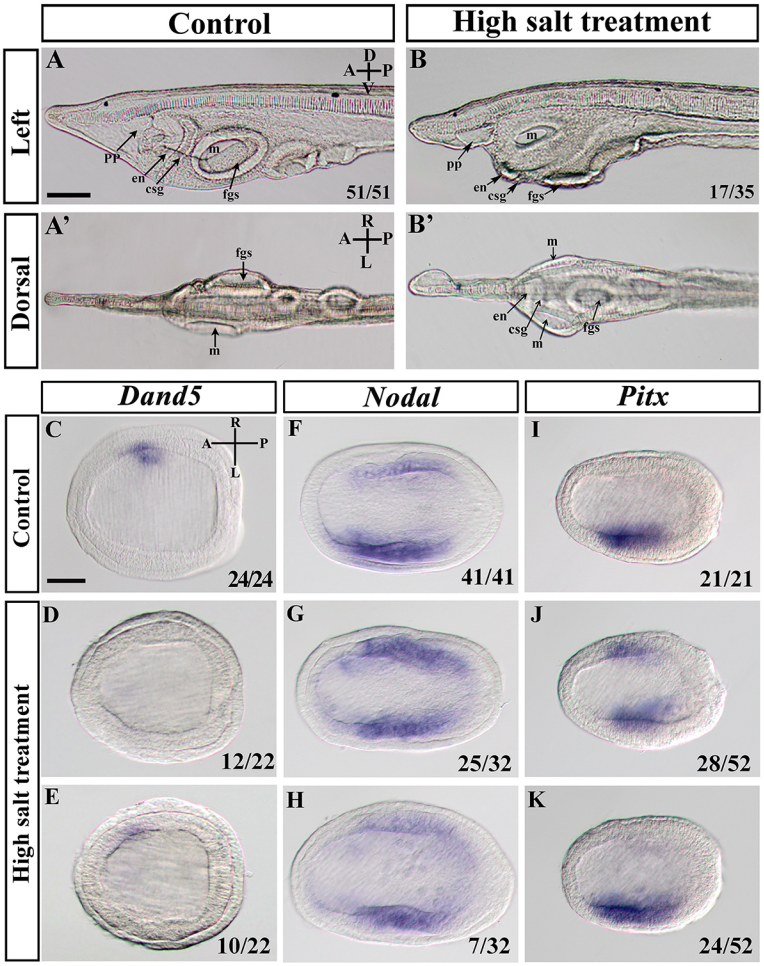

Fig. 5. Removal of the cilia by high-salt seawater treatment impairs L-R asymmetric morphology and Dand5-Nodal cascade induction. (A,A′) Asymmetric morphology of a control larva. Left lateral view of the pharyngeal region focused on the right side (A), showing the left-side pre-oral pit (pp), right-side endostyle (en) and club-shaped gland (csg). Dorsal view of the pharyngeal region focused on the ventral side (A′), showing the left-side mouth (m) and the right-side first gill slit (fgs). (B,B′) Left-isomerism morphology in the high-salt treatment larvae. Left lateral view of the pharyngeal region with focus on the sagittal plane (B), showing the left-side pp, and en, csg and fgs on the ventral side. Dorsal view of the pharyngeal region focused on the ventral side (B′), showing duplication of the mouth, ventral portion of the en and duct of the csg. (C-E) Expression patterns of *Dand5* in the control and HS-treated embryos at the early neurula stage. (F-H) Expression patterns of *Nodal* in the control and HS-treated embryos at the five-somite stage. (I-K) Expression patterns of *Pitx* in the control and HS-treated embryos at the two-somite stage. Images in C-K were taken from the dorsal view with the anterior to the left. Numbers in the bottom right corner of a panel show the number of times the phenotype was observed in the total number of embryos examined. A, anterior; D, dorsal; L, left side; P, posterior; R, right side; V, ventral. Scale bar: 50 µm in A (for A-B′) and in C (for C-K).

transfers Hh protein from the anterior axial mesoderm, in which it is synthesized and secreted, preferentially to the anterior-right paraxial mesoderm. This right-biased Hh protein causes asymmetric Hh signalling and further induces *Dand5* expression in the anterior-right paraxial mesodermal cells. However, it is still unknown whether Hh signalling regulates *Dand5* transcription directly or not. A canonical binding element for the Hh signalling transcription factor *Gli* has been deduced in the upstream region of the *Dand5* transcription initiation site (Hu et al., 2017). However, the element does not appear to be essential for *Dand5* transcription, as amphioxus embryos without it (Fig. S15A) show normal *Dand5* expression and L-R patterns (Fig. S15C,D). Nevertheless, the result does not exclude the possibility that Hh signalling regulates *Dand5* expression directly, as other Gli-binding sites in the *Dand5* promoter may exist.

The Hh signalling pathway is one of the key pathways that is essential for metazoan embryonic development. Its involvement in L-R asymmetry has been reported in mice, chickens and sea urchins (Meyers and Martin, 1999; Tsukui et al., 1999; Zhang et al., 2001; Levin et al., 1995; Warner et al., 2016). In chicken, *Shh* is expressed to the left of Hensen's node, where it functions as a left determinant by inducing asymmetric expression of *Nodal* and *Pitx* genes in the left side of the embryo (Levin et al., 1995). In contrast, in mice, *Shh* is bilaterally expressed in either the node or in other regions of the embryo, and knocking it out leads to the bilateral expression of the *Nodal*, *Lefty2* and *Pitx* genes (Meyers and Martin, 1999; Tsukui et al., 1999). According to this finding, Meyers and Martin (1999) suggested that Shh acts as a right determinant by repressing the expression of left determinants on the right side, whereas Tsukui et al. (1999) posited that Shh is required to establish a physical barrier in the midline that prevents the spread of left determinants to the right side. Consistent with the latter idea, the expression of the Nodal inhibitor Lefty1 in the midline is lost in $Shh^{-/-}$ embryos (Tsukui et al., 1999). A later study revealed that the involvement of Hh signalling in mouse L-R asymmetry development is achieved by maintaining and propagating Nodal expression in the lateral plate mesoderm (Tsiairis and McMahon, 2009). Similar to that in mice, Hh signalling in sea urchins is required to maintain and propagate late-phase Nodal signalling activity (Warner et al., 2016). However, the necessity of Hh signalling for L-R formation has not been demonstrated in zebrafish, as zebrafish mutants lacking Shh, Smo and/or other signalling components show normal L-R morphogenesis (Schauerte et al., 1998; Chen et al., 2001), although mis-expression of the *Shh* gene in zebrafish embryos causes L-R patterning defects (Schilling et al., 1999). We have previously shown that the Hh signalling pathway is required for amphioxus L-R asymmetry development because it controls *Dand5* expression (Hu et al., 2017). In this study, we provide further evidence that Hh signalling is asymmetrically activated (L<R), which might provide an initial cue for asymmetric *Dand5* expression in amphioxus embryos.

As discussed above, the mechanism by which Hh signalling regulates L-R asymmetry development in amphioxus appears to be different from that in other deuterostomes. However, it should

Development (2020) 147, dev182469. doi:10.1242/dev.182469

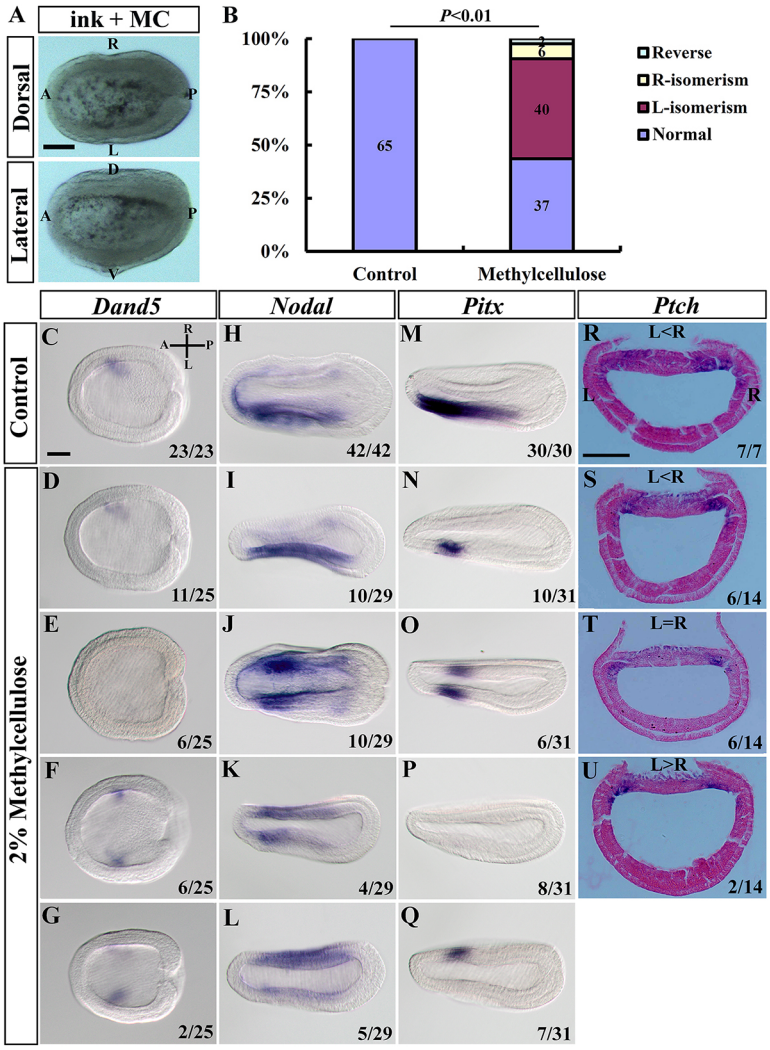

Fig. 6. Methylcellulose treatment affects L-R asymmetric development and asymmetric gene expression in amphioxus. (A) Treatment of embryos from the mid-gastrula to the N1 neurula stage with black ink-coloured methylcellulose (MC). (B) Quantification of embryos showing left-right asymmetric (normal), right-isomerism, left-isomerism and reversed phenotypes. The numbers in the column represent the number of each phenotype observed. (C-G) Expression patterns of *Dand5* in the control (C) and MC-treated (D-G) embryos at the early neurula stage. (H-L) Expression patterns of *Nodal* in the control (H) and MC-treated (I-L) embryos at the five-somite stage. (M-Q) Expression patterns of *Pitx* in the control (M) and MC-treated (N-Q) embryos at the five-somite stage. Images in C-Q were taken from the dorsal view with the anterior to the left, and show representative images of each phenotype. (R-U) Expression patterns of *Ptch* in the control (R) and MC-treated (S-U) embryos at the early neurula stage. Images R-U are visualized by transverse section. Numbers in the bottom right corner of a panel show the number of times the phenotype was observed in the total number of embryos examined. A, anterior; D, dorsal; L, left side; P, posterior; R, right side; V, ventral. Scale bar: 50 µm in A, C (for C-G) and R (for R-U).

be noted that NVPs containing the Shh protein have also been shown to be asymmetrically transported across the nodes of mouse embryos (Tanaka et al., 2005). It is currently unclear whether asymmetric Shh distribution in the mouse node is crucial for transducing nodal flow signal to induce asymmetric *Dand5* or *Nodal* expression, as no mouse mutants conditionally lacking Hh signalling activity in the LRO have been analyzed. Mice have multiple paralogous genes with redundant roles for most members of the Hh signalling pathway, and Hh signalling can regulate L-R patterning in mice at different levels, as explained above. These complex networks make examining the Hh signalling function in the mouse LRO extremely difficult. For sea urchin embryos, which have a single *Hh* gene (Walton et al., 2006), the involvement of Hh signalling in *Nodal* expression regulation in the right-side ectoderm (late phase) has been demonstrated using morpholino, cyclopamine (a Smo inhibitor) and antibody (against kinesin-II, to block ciliogenesis)-mediated knockdown methods (Warner et al., 2016). However, this study does not necessarily preclude the possibility that Hh signalling can regulate the early phase of *Nodal* expression in the tip of the archenteron, as incomplete loss-of-function and nonspecific effects from the use of the methods described above may have had an influence. Interestingly, *Ptch* and *Smo* are co-expressed in the archenteron of sea urchin embryos, similarly to *Nodal* (Warner et al., 2014, 2016), which makes the above speculation more reasonable. Therefore, more studies are needed to reveal whether Hh signalling regulates asymmetric *Dand5* expression or *Nodal* expression in species in addition to amphioxus in the future.

Bilateral symmetry breaking of vertebrate embryos relies on cilia-driven nodal fluid flow at the L-R organizer (Okada et al., 2005; Schweickert et al., 2007; Tabin and Vogan, 2003). The timing of the initial cilium incorporation into the L-R asymmetry is an area of interest to developmental biologists. A recent study found that cells in the archenteron possess motile cilia in sea urchin embryos, and the removal of the cilia using HS seawater resulted in abnormal *Nodal* expression and L-R defects (Tisler et al., 2016). Similarly, in ascidian *H. roretzi*, blocking neurula rotation driven by the motile cilia also disrupts asymmetric *Nodal* expression and L-R morphology (Nishide et al., 2012). In the sea urchin and *H. roretzi*, no *Dand5* genes have been identified, and *Nodal* is the earliest gene asymmetrically expressed. Amphioxus embryos are heavily ciliated from the gastrula stage (Hirakow and Kajita, 1991). At the early neurula stage, the cilia begin to beat and drive the embryo to rotate within the fertilization envelope. We showed that removing cilia or blocking cilia movement in amphioxus embryos from the late mid-gastrula (G4) to the early neurula stages disrupts the asymmetric activation of Hh signalling and *Dand5* expression. Given that amphioxus embryo rotation occurs after asymmetric *Dand5* and *Ptch* expression is first detected and that blocking embryo rotation (without disturbing cilia movement) does not significantly affect L-R patterning, we speculate that cilia

Development (2020) 147, dev182469. doi:10.1242/dev.182469

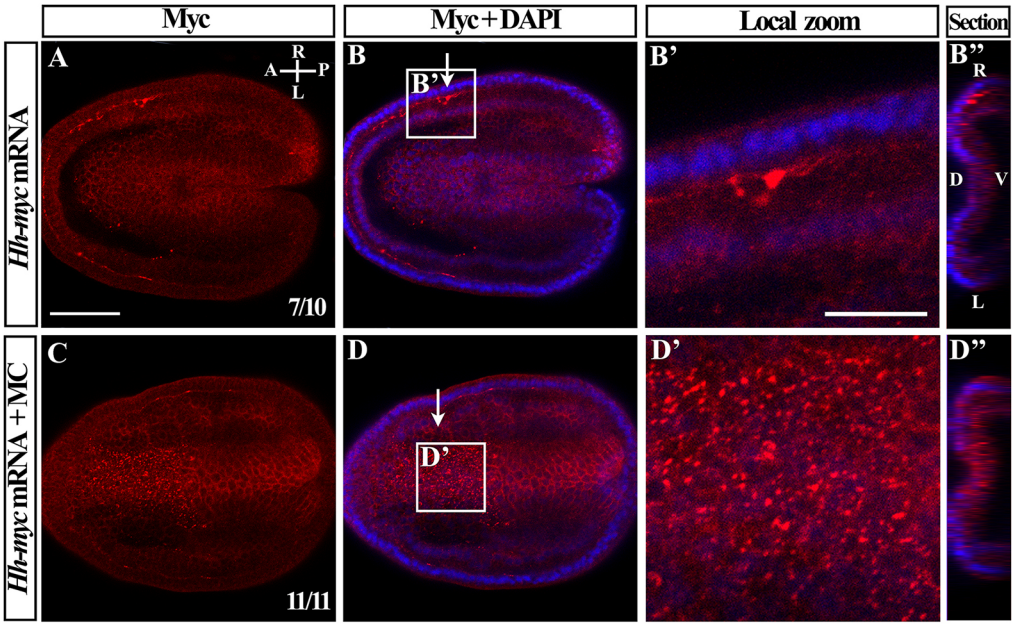

Fig. 7. Methylcellulose treatment inhibits right-bias transportation of the Hh fusion protein in amphioxus. (A-D″) Immunofluorescence images of the Hh-Myc fusion protein and cell nucleus. Hh-Myc fusion protein is detected by the Myc antibody (red) and the cell nuclei are labelled with DAPI (blue). A right-bias distribution of the Hh fusion protein in the paraxial mesoderm was detected in the *Hh-myc* mRNA-injected embryos at the early neurula stage (A,B). Hh fusion protein was present mainly in midline tissue without apparent laterality in methylcellulose (MC)-treated embryos (C,D). B′ and D′ show a magnification of the white boxed area in B and D, respectively. B″ and D″ show section planes at the levels indicated in B and D, respectively (arrows). Images in A-D were taken from the dorsal view with the anterior to the left. Numbers in the bottom right corner of a panel show the number of times the phenotype was observed in the total number of embryos examined. A, anterior; D, dorsal; L, left side; P, posterior; R, right side; V, ventral. Scale bar: 50 µm in A (for A-D,B″,D″); 20 µm in B′ (for B′,D′).

movement, but not embryo rotation, is responsible for amphioxus symmetry breaking. Together, these findings indicate that the involvement of motile cilia in symmetry breaking most likely emerged, at least, before the divergence of deuterostomes.

Although nodal flow was first identified in mouse embryos in 1998 (Nonaka et al., 1998), the mechanism by which nodal flow affects L-R patterning remains unclear. Several models have been proposed to explain this process, two of which (the two-cilia model and the morphogen model) have attracted the most attention. The two-cilia model posits that the motile cilia within the node generate the flow and the immotile cilia at the node edge sense the mechanical force from the flow. The morphogen model suggests that the nodal flow transports a certain substance called a morphogen preferentially to the left side of the node, which is then sensed by the morphogen receptors to initiate expression of the left-side genes such as *Nodal*, *Lefty* and *Pitx2* (Tabin and Vogan, 2003). Consistent with the two-cilia model, Yoshiba et al. showed that the immotile cilia of perinodal crown cells could sense the flow in a Ca^{2+} channel protein (e.g. Pkd2)-dependent manner to induce the asymmetric expression of *Cerl2* and *Nodal* in the node (Yoshiba et al., 2012). However, this finding could also be interpreted as evidence for the morphogen hypothesis, as the targets sensed by the immotile cilia can be either a mechanical force or a morphogen. Indeed, Tanaka et al. showed that the addition of recombinant Shh or Indian hedgehog into the embryo culture medium could elevate the left-specific Ca^{2+} level that had been suppressed by blocking FGF signalling (Tanaka et al., 2005). This suggests a role for Hh signalling in triggering an initial asymmetric Ca^{2+} elevation on the left side. Our findings in the present study, however, favour a combination of these two models. We showed that cilia of the amphioxus embryos were not only involved in transporting the Hh protein (morphogen) preferentially to the anterior-right paraxial mesoderm, but also required for Hh signal transduction. These two actions of the cilia eventually result in R>L Hh signalling and *Dand5* expression in the anterior-right paraxial mesoderm. Surprisingly, we did not detect an obvious Hh fusion protein in the apical (ventral) side of the axial mesoderm or in the right paraxial mesoderm. The possible explanation for this is that the Hh protein in these domains was washed out during the WIF analysis, or the asymmetric Hh distribution may be an indirect consequence of cilia movement. As all cilia present in early neurulae, including those on the neural ectodermal cell on which caSmo is predominantly detected, are motile (see discussion below and Movie 3), we speculated that the cilia responsible for Hh signal transduction in amphioxus embryos are motile, similar to those in the sea urchin embryos (Warner et al., 2014).

The LRO in vertebrate and sea urchin embryos is derived from mesoderm and is the first place at which asymmetric gene expression occurs (Nakamura and Hamada, 2012; Tisler et al., 2016). Cells in the LRO also have motile monocilia, with an average length of 5 µm, which rotate to generate nodal flow (Okada et al., 2005; Schweickert et al., 2007). In amphioxus, the earliest asymmetric signals (such as those associated with Hh distribution, or *Dand5* and *Ptch* expression) occur in the anterior-right mesoderm, which suggests that the GRP (mesoderm-derived) located between the anterior paraxial mesoderm in early amphioxus neurulae might be analogous to the vertebrate LRO (Li et al., 2017; Blum et al., 2014). However, monocilia on most GRP cells of the amphioxus embryo of the four sequential stages (from the G5 stage to 90 min after this stage) are much longer (~10 µm) than those on the vertebrate LRO (Fig. S16), and they do not rotate; they only beat very weakly (Movie 3). We also tried to determine whether a unidirectional flow can be found at the GRP region by adding fluorescent beads to the GRP explant, but this experiment failed because the beads always gathered into large masses in the sea water (Fig. S17). Monocilia on the NE cells in early neurulae are of similar length (2-5 µm) to those on the

Development (2020) 147, dev182469. doi:10.1242/dev.182469

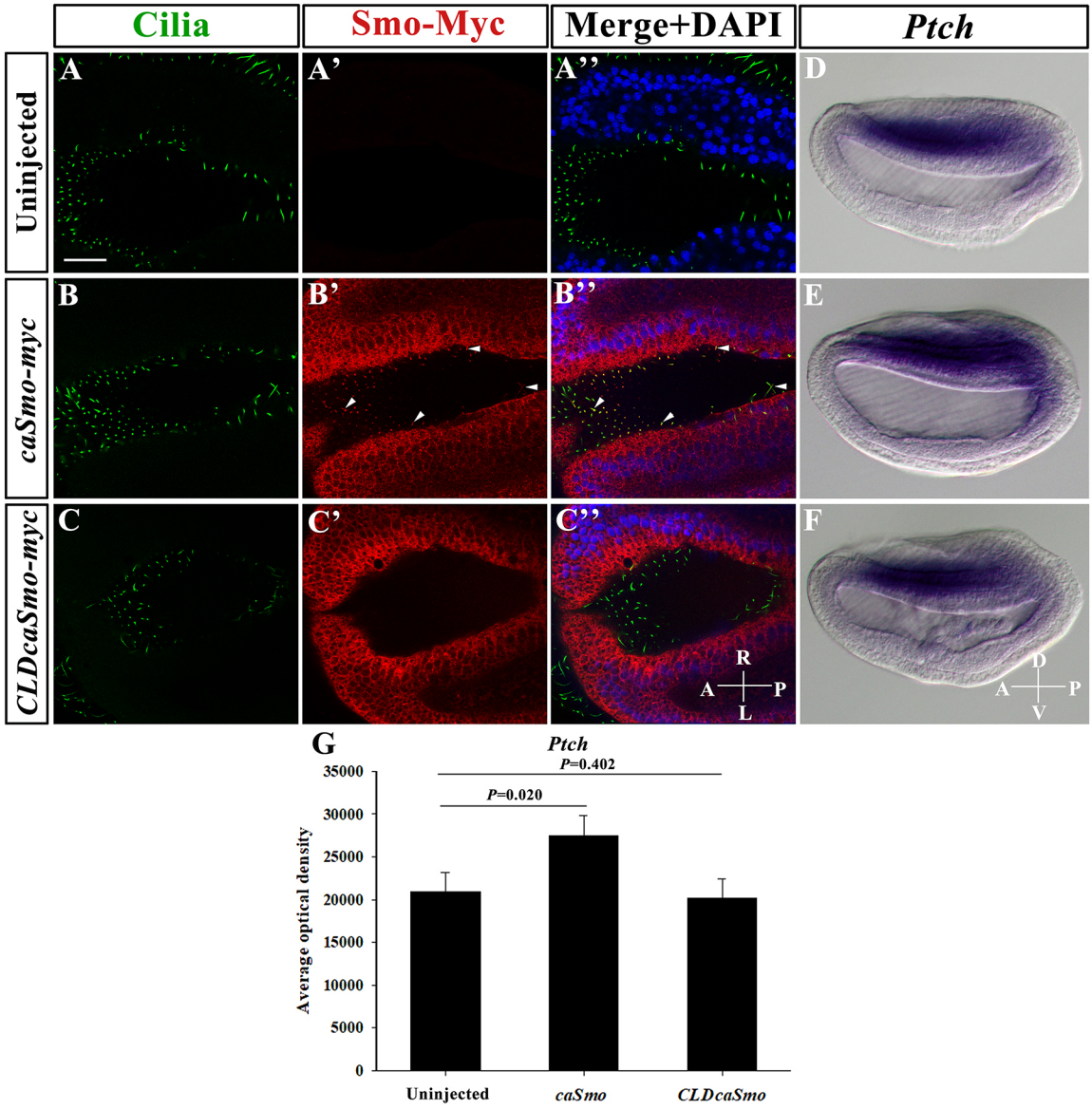

Fig. 8. caSmo-Myc fusion protein localizes to cilia. (A-A″) Immunofluorescence images of the uninjected embryos at the early neurula stage, showing that no Myc fusion protein (red) localized to the cilia (acetylated tubulin antibody, green). (B-B″) Immunofluorescence images of the *caSmo-myc* mRNA-injected embryos, showing that the Myc fusion protein localized to the cilia. White arrowheads indicate the cilia localization of the caSmo fusion protein. (C-C″) Immunofluorescence images of the CLD*caSmo-myc* mRNA-injected embryos, showing that no Myc fusion protein localized to the cilia but did localize to the cytoplasm. Cell nuclei are stained with DAPI (blue). (D-G) The expression of *Ptch* in uninjected, *caSmo-myc* mRNA- and *CLDcaSmo-myc* mRNA-injected embryos, showing that *Ptch* expression is increased in the *caSmo-myc* mRNA-injected embryos. However, there was no difference between the uninjected and *CLDcaSmo-myc* mRNA-injected embryos. A, anterior; D, dorsal; L, left side; P, posterior; R, right side; V, ventral. Scale bar: 20 µm in A (for A-F).

vertebrate LRO, but they also move differently (they beat but do not rotate; Movie 3). The last class of monocilia observed in amphioxus early neurulae are those on EE cells; however, they also beat but not rotate and are longer than the cilia on the vertebrate LRO. Therefore, none of the three types of monocilia found in amphioxus embryos satisfies every criteria to match the cilia of the vertebrate LRO. This leaves unanswered the questions about whether the amphioxus embryo has an LRO-like structure and its possible position.

Taken together, our data show that motile cilia are essential for symmetry breaking in amphioxus through the asymmetric transport of Hh protein and the transduction of related asymmetric signals to induce asymmetric *Dand5* expression. Therefore, cilia-driven symmetry breakage likely represents an evolutionarily conserved mechanism in deuterostomes.

MATERIALS AND METHODS

Animal cultivation, mutant generation and genotyping

Amphioxus (*Branchiostoma floridae*) were obtained from a stock maintained by Dr Jr-Kai Yu (Institute of Cellular and Organismic Biology, Academia Sinica, Taipei, Taiwan) and raised under previously described conditions (Li et al., 2012). Gametes were obtained by thermal shock (Li et al., 2013); embryos were raised as previously described (Liu et al., 2013). *Hh* mutants were generated as described in a previous report (Wang et al., 2015). *Kif3a*, *Foxj1* and *Dand5* mutants were generated using the TALEN method as previously described (Li et al., 2014, 2017). Homozygous mutants were generated by crossing the heterozygous animals. Genotyping of the live embryos was performed as previously described (Li et al., 2017), and genotyping of the embryos fixed with fixative was conducted with the same protocol except an extra 30 min wash in 500 ml of filtered sea water or PBS was added before lysis to remove the fixative. All embryos were

Development (2020) 147, dev182469. doi:10.1242/dev.182469

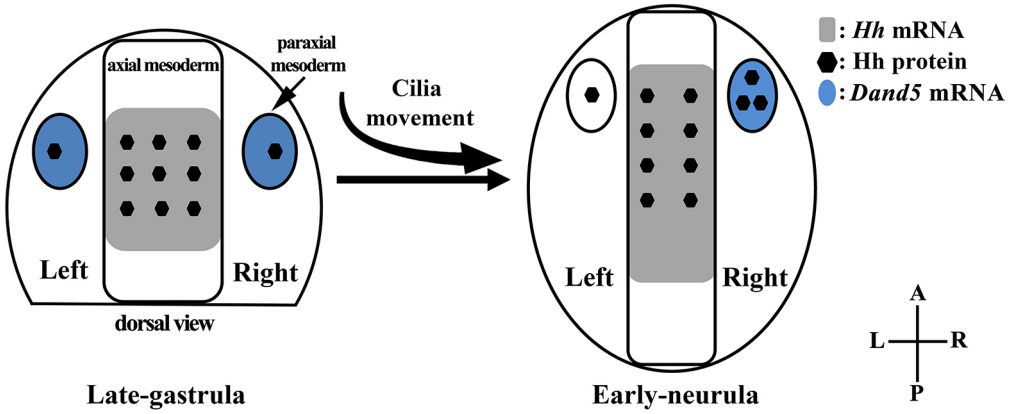

Fig. 9. A model for cilia and asymmetric Hh signalling in the control of amphioxus L-R asymmetry. At the late gastrula/G5 stage, in which cilia movement is lacking or weak, the Hh protein is synthesized and secreted in the midline region and spreads symmetrically (likely by diffusion) to the left and right side of the anterior paraxial mesoderm, in which symmetric *Dand5* expression is induced. During the early neurula stage, in which cilia movement is apparent, the Hh protein from the midline region is transported dominantly to the right paraxial mesoderm by cilia movement, leading to R>L Hh signalling and *Dand5* expression in the paraxial mesoderm. A, anterior; L, left side; P, posterior; R, right side.

staged according to the naming system described in Hirakow and Kajita (1991; 1994), unless otherwise stated. Primers adopted for gene fragment amplification are shown in Table S1.

Construct preparation, mRNA synthesis and embryo microinjection

Coding sequences of the *Smo* and *Hh* genes were amplified from cDNA libraries based on amphioxus embryos. PCR products were cloned into the pGEM-T-Easy vector (Promega) for probe synthesis or into the pXT7 vector for mRNA synthesis. A G-to-T mutation at the 1556 bp site downstream of the *Smo* start codon (resulting in a Trp-to-Leu change) was made to construct a constitutively active form of the protein according to the method of Xie et al. (1998) using PCR. A 6×*myc* tag was fused to the C terminus of the *Hh* and to the *caSmo* coding sequences using a Gibson assembly cloning kit (New England Biolabs). A form of caSmo (*CLD*ca*Smo*) with a defective ciliary localization motif was constructed according to Huangfu et al. (2003) using the PCR method. All constructs were confirmed using DNA sequencing. *In vitro* mRNA synthesis was conducted using a T7 mMESSAGE mMACHINE kit (Ambion). The primers used in the vector constructs described above are shown in Table S1.

Unfertilized eggs were injected and fertilized as previously described (Liu et al., 2013). For blastomere injection at the two-cell stage, embryos were de-enveloped ∼20 min after fertilization with a finely pulled plastic Pasteur dropper and then transferred at the two-cell stage to a 3 cm×4 cm coverslip coated with 4 µl 0.025 mg/ml polylysine. The injection was conducted essentially in a manner identical to the injection of an unfertilized egg. Embryos injected on the left side or right side were separated at the G5 stage and visualized under a fluorescence stereomicroscope (Olympus, SZX10).

WISH, histological and immunofluorescence analyses

Embryos at the desired developmental stages were fixed overnight with 4% PFA-MOPS-EGTA (wt/vol) at 4°C, transferred into 70% ethanol (vol/vol) and maintained at −20°C for use. *Smo* or *Gli* digoxigenin (DIG)-labelled antisense riboprobes (Roche) were synthesized with Sp6 or T7 RNA polymerase (Promega). *Hh*, *Ptc*, *Dand5*, *Nodal*, *Lefty* and *Pitx* RNA probes were generated as previously described (Li et al., 2017; Hu et al., 2017). WISH was performed as previously described (Yu and Holland, 2009). The stained embryos were photographed under an inverted microscope (Olympus, IX71), or they were embedded in agar-paraffin, sectioned to a thickness of 6 µm and photographed under an upright microscope (Zeiss, AX10).

For Myc or acetylated tubulin staining, the embryos were blocked in a solution containing 5% goat serum, 0.1% Triton X-100 and 0.1% bovine serum albumin (BSA) in PBS for 1 h and incubated overnight with a primary antibody against Myc (Santa Cruz Biotechnology, 9E10, 1:100) or acetylated tubulin (Sigma-Aldrich, T7451, 1:1000 or Cell Signaling Technology, 5335, 1:1000) at 4°C. Immunofluorescence signals were detected with a secondary antibody (Alexa Fluor 594-conjugated goat anti-mouse antibody, A-11032, or Alexa Fluor 488-conjugated goat anti-rabbit antibody, A-11034, Invitrogen, 1:400). DAPI (Solarbio, D8200, 1 µg/ml in PBST) was adopted for nuclear staining. Fluorescent images were acquired using a confocal microscope (Zeiss, LSM780).

Electron microscopy observations

Embryos for scanning electron microscopy were fixed overnight with fresh 2.5% glutaraldehyde in filtered seawater at 4°C, washed 3×10 min in 0.1 M PBS (pH 7.4), and dehydrated in an ethanol series to 100% ethanol. Samples were then dried using the critical point drying method, sprayed with platinum, placed on conductive tape, and observed under a JSM-6390 scanning microscope (JEOL).

The embryos used for immunoelectron microscopy were fixed overnight with 4% PFA-MOPS-EGTA at 4°C, dehydrated in an ethanol series, embedded in LR White resin (Sigma-Aldrich, 62661) and sectioned at 70 nm. The sections were washed 3× in 0.01 M PBS (pH 7.4), blocked in a solution containing 1% BSA, 0.05% Triton X-100, 0.05% Tween 20 in 0.01 M PBS (pH 7.4) for 20 min and incubated overnight with primary antibody against Myc (Santa Cruz Biotechnology, 9E10, 1:100) at 4°C. After being washed with ddH_2O, the sections were incubated with goat-anti-mouse IgG antibody conjugated with 10 nm colloidal gold (Electron Microscopy Sciences, 25128, 1:50) for 3 h, washed with ddH_2O, post-fixed in 2.5% glutaraldehyde in PBS (pH 7.4), stained in 2% uranyl acetate (pH 5.1) and observed under a Hitachi HT-7800 transmission electron microscope.

Embryo treatments with HS seawater or MC

Embryos were de-enveloped at the G4 stage (late mid-gastrula stage) and then treated with 0.83 M NaCl seawater for 60-90 s to remove the cilia. As the embryos can recover cilia very quickly, they were also treated every 15-20 min until they reached the N1 stage. For the MC treatment, the embryos were de-enveloped at the G4 stage and then cultured in filtered seawater containing 2% MC (wt/vol) until R30 (half-hour after the initial neurula rotation stage) or the five-somite stage.

Inhibition of neurula rotation

The embryos were de-enveloped at G4 stage, moved to seawater containing 0.5% MC (wt/vol) and threaded through a very fine glass needle and mounted on glass slides with double-sided foam adhesive (as shown in Fig. S12). They were released and transferred to filtered seawater at the three-somite stage and analyzed at the desired stages.

Observation of cilia motility

Embryos were de-enveloped at the G5 stage and cut with injection needles to obtain explants. The embryos or explants were then transferred to a 35-mm glass-bottom dish with 20-mm micro-wells filled with seawater containing 0.5% MC, and they were observed under a Zeiss Axio Imager 2 Research Microscope or a precision DeltaVision-OMX Super-Resolution Microscope (GE OMX V4).

Quantification and statistical analysis

The average optical density of the *in situ* hybridization signal was evaluated using Image-Pro Plus 6.0 software (Media Cybernetics). Cilia length statistics were determined using Image-Pro Plus 6.0 software. Significance was calculated using independent samples *t*-tests or a Fisher exact test with IBM SPSS Statistics version 19 (IBM Corporation).

Acknowledgements

We thank Dr Sebastian Shimeld for his helpful comments and language editing on the manuscript, Dr Chengtian Zhao for providing us with the acetylated tubulin antibody, and the three anonymous reviewers for their critical comments on the manuscript. We are grateful that Dr Luming Yao and Dr Caiming Wu helped us with sample preparation and electron microscopy observation and Dr Qingfeng Liu assisted us in confocal microscope observation.

Competing interests

The authors declare no competing or financial interests.

Author contributions

Conceptualization: Y.W., G.L.; Methodology: X.Z., G.L.; Validation: X.Z., Y.W., G.L.; Formal analysis: X.Z., C.S., Y.Z., X.L., Y.W., G.L.; Investigation: X.Z., C.S., Y.Z., X.L., Q.Y., X.W., G.L.; Data curation: X.Z., C.S., Y.Z., X.L., Y.W., G.L.; Writing - original draft: X.Z., Y.W., G.L.; Writing - review & editing: X.Z., Y.W., G.L.; Visualization: G.L.; Supervision: Y.W., G.L.; Project administration: G.L.; Funding acquisition: Y.W., G.L.

Funding

The work is supported by grants from the National Natural Science Foundation of China (31672246, 31872186 and 31471986) and Fundamental Research Funds for the Central Universities, China (20720160056).

Supplementary information

Supplementary information available online at
http://dev.biologists.org/lookup/doi/10.1242/dev.182469.supplemental

References

Aldea, D., Leon, A., Bertrand, S. and Escriva, H. (2015). Expression of Fox genes in the cephalochordate *Branchiostoma lanceolatum*. *Front. Ecol. Evol.* **3**, 80. doi:10.3389/fevo.2015.00080

Auclair, W. and Siegel, B. W. (1966). Cilia regeneration in the sea urchin embryo: evidence for a pool of ciliary proteins. *Science* **154**, 913-915. doi:10.1126/science.154.3751.913

Blum, M., Weber, T., Beyer, T. and Vick, P. (2009). Evolution of leftward flow. *Semin. Cell Dev. Biol.* **20**, 464-471. doi:10.1016/j.semcdb.2008.11.005

Blum, M., Feistel, K., Thumberger, T. and Schweickert, A. (2014). The evolution and conservation of left-right patterning mechanisms. *Development* **141**, 1603-1613. doi:10.1242/dev.100560

Chen, W., Burgess, S. and Hopkins, N. (2001). Analysis of the zebrafish smoothened mutant reveals conserved and divergent functions of hedgehog activity. *Development* **128**, 2385-2396.

Delling, M., Indzhykulian, A. A., Liu, X., Li, Y., Xie, T., Corey, D. P. and Clapham, D. E. (2016). Primary cilia are not calcium-responsive mechanosensors. *Nature* **531**, 656-660. doi:10.1038/nature17426

Essner, J. J., Amack, J. D., Nyholm, M. K., Harris, E. B. and Yost, H. J. (2005). Kupffer's vesicle is a ciliated organ of asymmetry in the zebrafish embryo that initiates left-right development of the brain, heart and gut. *Development* **132**, 1247-1260. doi:10.1242/dev.01663

Ferreira, R. R., Vilfan, A., Jülicher, F., Supatto, W. and Vermot, J. (2017). Physical limits of flow sensing in the left-right organizer. *eLife* **6**, e25078. doi:10.7554/eLife.25078

Grimes, D. T. and Burdine, R. D. (2017). Left-right patterning: breaking symmetry to asymmetric morphogenesis. *Trends Genet.* **33**, 616-628. doi:10.1016/j.tig.2017.06.004

Hashimoto, H., Rebagliati, M., Ahmad, N., Muraoka, O., Kurokawa, T., Hibi, M. and Suzuki, T. (2004). The Cerberus/Dan-family protein Charon is a negative regulator of Nodal signaling during left-right patterning in zebrafish. *Development* **131**, 1741-1753. doi:10.1242/dev.01070

Hirakow, R. and Kajita, N. (1991). Electron microscopic study of the development of amphioxus, *Branchiostoma belcheri tsingtauense*: The gastrula. *J. Morphol.* **207**, 37-52. doi:10.1002/jmor.1052070106

Hirakow, R. and Kajita, N. (1994). Electron microscopic study of the development of amphioxus, *Branchiostoma belcheri tsingtauense*: the neurula and larva. *Kaibogaku zasshi. J. Anat.* **69**, 1-13.

Holland, P. W., Koschorz, B., Holland, L. Z. and Herrmann, B. G. (1995). Conservation of *Brachyury* (T) genes in amphioxus and vertebrates: developmental and evolutionary implications. *Development* **121**, 4283-4291.

Holland, L. Z., Laudet, V. and Schubert, M. (2004). The chordate amphioxus: an emerging model organism for developmental biology. *Cell. Mol. Life Sci.* **61**, 2290-2308. doi:10.1007/s00018-004-4075-2

Hooper, J. E. and Scott, M. P. (2005). Communicating with Hedgehogs. *Nat. Rev. Mol. Cell Biol.* **6**, 306-317. doi:10.1038/nrm1622

Hu, G., Li, G., Wang, H. and Wang, Y. (2017). Hedgehog participates in the establishment of left-right asymmetry during amphioxus development by controlling Cerberus expression. *Development* **144**, 4694-4703. doi:10.1242/dev.157172

Huangfu, D., Liu, A., Rakeman, A. S., Murcia, N. S., Niswander, L. and Anderson, K. V. (2003). Hedgehog signalling in the mouse requires intraflagellar transport proteins. *Nature* **426**, 83-87. doi:10.1038/nature02061

Lee, J., Platt, K. A., Censullo, P. and i Altaba, A. R. (1997). Gli1 is a target of Sonic hedgehog that induces ventral neural tube development. *Development* **124**, 2537-2552.

Levin, M., Johnson, R. L., Sterna, C. D., Kuehn, M. and Tabin, C. (1995). A molecular pathway determining left-right asymmetry in chick embryogenesis. *Cell* **82**, 803-814. doi:10.1016/0092-8674(95)90477-8

Li, G., Yang, X., Shu, Z. H., Chen, X. Y. and Wang, Y. Q. (2012). Consecutive spawnings of Chinese amphioxus, *Branchiostoma belcheri*, in captivity. *PLoS One* **7**, e50838. doi:10.1371/journal.pone.0050838

Li, G., Shu, Z. H. and Wang, Y. Q. (2013). Year-round reproduction and induced spawning of Chinese amphioxus, *Branchiostoma belcheri*, in laboratory. *PLoS One* **8**, e75461. doi:10.1371/journal.pone.0075461

Li, G., Feng, J., Lei, Y., Wang, J., Wang, H., Shang, L.-K., Liu, D.-T., Zhao, H., Zhu, Y. and Wang, Y.-Q. (2014). Mutagenesis at specific genomic loci of amphioxus *Branchiostoma belcheri* using TALEN method. *J. Genet. Genomics* **41**, 215-219. doi:10.1016/j.jgg.2014.02.003

Li, G., Liu, X., Xing, C. F., Zhang, H. Y., Shimeld, S. M. and Wang, Y. Q. (2017). Cerberus–Nodal–Lefty–Pitx signaling cascade controls left-right asymmetry in amphioxus. *Proc. Natl. Acad. Sci. U.S.A.* **114**, 3684-3689. doi:10.1073/pnas.1620519114

Liu, X., Li, G., Feng, J., Yang, X. and Wang, Y.-Q. (2013). An efficient microinjection method for unfertilized eggs of Asian amphioxus *Branchiostoma belcheri*. *Dev. Genes Evol.* **223**, 269-278. doi:10.1007/s00427-013-0441-0

Marszalek, J. R., Ruiz-Lozano, P., Roberts, E., Chien, K. R. and Goldstein, L. S. B. (1999). Situs inversus and embryonic ciliary morphogenesis defects in mouse mutants lacking the KIF3A subunit of kinesin-II. *Proc. Natl. Acad. Sci. USA* **96**, 5043-5048. doi:10.1073/pnas.96.9.5043

McGrath, J., Somlo, S., Makova, S., Tian, X. and Brueckner, M. (2003). Two populations of node monocilia initiate left-right asymmetry in the mouse. *Cell* **114**, 61-73. doi:10.1016/S0092-8674(03)00511-7

Meyers, E. N. and Martin, G. R. (1999). Differences in left-right axis pathways in mouse and chick: functions of FGF8 and SHH. *Science* **285**, 403-406. doi:10.1126/science.285.5426.403

Nakamura, T. and Hamada, H. (2012). Left-right patterning: conserved and divergent mechanisms. *Development* **139**, 3257-3262. doi:10.1242/dev.061606

Nakamura, T., Saito, D., Kawasumi, A., Shinohara, K., Asai, Y., Takaoka, K., Dong, F., Takamatsu, A., Belo, J. A., Mochizuki, A. et al. (2012). Fluid flow and interlinked feedback loops establish left-right asymmetric decay of Cerl2 mRNA. *Nat. Commun.* **3**, 1322. doi:10.1038/ncomms2319

Nishide, K., Mugitani, M., Kumano, G. and Nishida, H. (2012). Neurula rotation determines left-right asymmetry in ascidian tadpole larvae. *Development* **139**, 1467-1475. doi:10.1242/dev.076083

Nonaka, S., Tanaka, Y., Okada, Y., Takeda, S., Harada, A., Kanai, Y., Kido, M. and Hirokawa, N. (1998). Randomization of left–right asymmetry due to loss of nodal cilia generating leftward flow of extraembryonic fluid in mice lacking KIF3B motor protein. *Cell* **95**, 829-837. doi:10.1016/S0092-8674(00)81705-5

Okada, Y., Takeda, S., Tanaka, Y., Belmonte, J.-C. I. and Hirokawa, N. (2005). Mechanism of nodal flow: a conserved symmetry breaking event in left-right axis determination. *Cell* **121**, 633-644. doi:10.1016/j.cell.2005.04.008

Palmer, A. R. (1996). From symmetry to asymmetry: phylogenetic patterns of asymmetry variation in animals and their evolutionary significance. *Proc. Natl. Acad. Sci. U.S.A.* **93**, 14279-14286. doi:10.1073/pnas.93.25.14279

Putnam, N. H., Butts, T., Ferrier, D. E. K., Furlong, R. F., Hellsten, U., Kawashima, T., Robinson-Rechavi, M., Shoguchi, E., Terry, A., Yu, J.-K. et al. (2008). The amphioxus genome and the evolution of the chordate karyotype. *Nature* **453**, 1064-1071. doi:10.1038/nature06967

Schauerte, H. E., Van Eeden, F. J., Fricke, C., Odenthal, J., Strahle, U. and Haffter, P. (1998). Sonic hedgehog is not required for the induction of medial floor plate cells in the zebrafish. *Development* **125**, 2983-2993.

Schilling, T. F., Concordet, J.-P. and Ingham, P. W. (1999). Regulation of left-right asymmetries in the zebrafish by Shh and BMP4. *Dev. Biol.* **210**, 277-287. doi:10.1006/dbio.1999.9214

Schweickert, A., Weber, T., Beyer, T., Vick, P., Bogusch, S., Feistel, K. and Blum, M. (2007). Cilia-driven leftward flow determines laterality in *Xenopus*. *Curr. Biol.* **17**, 60-66. doi:10.1016/j.cub.2006.10.067

Schweickert, A., Vick, P., Getwan, M., Weber, T., Schneider, I., Eberhardt, M., Beyer, T., Pachur, A. and Blum, M. (2010). The nodal inhibitor coco is a critical target of leftward flow in *Xenopus*. *Curr. Biol.* **20**, 738-743. doi:10.1016/j.cub.2010.02.061

Shimeld, S. M. (2000). An amphioxus netrin gene is expressed in midline structures during embryonic and larval development. *Dev. Genes. Evol.* **210**, 337-344. doi:10.1007/s004270000073

Shinohara, K., Kawasumi, A., Takamatsu, A., Yoshiba, S., Botilde, Y., Motoyama, N., Reith, W., Durand, B., Shiratori, H. and Hamada, H. (2012). Two rotating cilia in the node cavity are sufficient to break left–right symmetry in the mouse embryo. *Nat. Commun.* **3**, 622. doi:10.1038/ncomms1624

Soukup, V. (2017). Left-right asymmetry specification in amphioxus: review and prospects. *Int. J. Dev. Biol.* **61**, 611-620. doi:10.1387/ijdb.170251vs

Sutherland, M. J. and Ware, S. M. (2009). Disorders of left–right asymmetry: Heterotaxy and situs inversus. *Am. J. Med. Genet. C Semin. Med. Genet.* **151C**, 307-317. doi:10.1002/ajmg.c.30228

Tabin, C. J. (2006). The key to left-right asymmetry. *Cell* **127**, 27-32. doi:10.1016/j.cell.2006.09.018

Tabin, C. J. and Vogan, K. J. (2003). A two-cilia model for vertebrate left-right axis specification. *Gene Dev.* **17**, 1-6. doi:10.1101/gad.1053803

Tamakoshi, T., Itakura, T., Chandra, A., Uezato, T., Yang, Z., Xue, X.-D., Wang, B., Hackett, B. P., Yokoyama, T. and Miura, N. (2006). Roles of the Foxj1 and Inv genes in the left–right determination of internal organs in mice. *Biochem. Biophys. Res. Commun.* **339**, 932-938. doi:10.1016/j.bbrc.2005.11.097

Tanaka, Y., Okada, Y. and Hirokawa, N. (2005). FGF-induced vesicular release of Sonic hedgehog and retinoic acid in leftward nodal flow is critical for left–right determination. *Nature* **435**, 172-177. doi:10.1038/nature03494

Tisler, M., Wetzel, F., Mantino, S., Kremnyov, S., Thumberger, T., Schweickert, A., Blum, M. and Vick, P. (2016). Cilia are required for asymmetric nodal induction in the sea urchin embryo. *BMC Dev. Biol.* **16**, 28. doi:10.1186/s12861-016-0128-7

Tsiairis, C. D. and McMahon, A. P. (2009). An Hh-dependent pathway in lateral plate mesoderm enables the generation of left/right asymmetry. *Curr. Biol.* **19**, 1912-1917. doi:10.1016/j.cub.2009.09.057

Tsukui, T., Capdevila, J., Tamura, K., Ruiz-Lozano, P., Rodriguez-Esteban, C., Yonei-Tamura, S., Magallon, J., Chandraratna, R. A. S., Chien, K., Blumberg, B. et al. (1999). Multiple left-right asymmetry defects in Shh(−/−) mutant mice unveil a convergence of the shh and retinoic acid pathways in the control of Lefty-1. *Proc. Natl. Acad. Sci. USA* **96**, 11376-11381. doi:10.1073/pnas.96.20.11376

Walton, K. D., Croce, J. C., Glenn, T. D., Wu, S.-Y. and Mcclay, D. R. (2006). Genomics and expression profiles of the Hedgehog and Notch signaling pathways in sea urchin development. *Dev. Biol.* **300**, 153-164. doi:10.1016/j.ydbio.2006.08.064

Wang, H., Li, G. and Wang, Y. Q. (2015). Generating amphioxus Hedgehog knockout mutants and phenotype analysis. *Hereditas* **37**, 1036-1043.

Warner, J. F., Mccarthy, A. M., Morris, R. L. and Mcclay, D. R. (2014). Hedgehog signaling requires motile cilia in the sea urchin. *Mol. Biol. Evol.* **31**, 18-22. doi:10.1093/molbev/mst176

Warner, J. F., Miranda, E. L. and Mcclay, D. R. (2016). Contribution of hedgehog signaling to the establishment of left–right asymmetry in the sea urchin. *Deve Biol* **411**, 314-324. doi:10.1016/j.ydbio.2016.02.008

Xie, J., Murone, M., Luoh, S.-M., Ryan, A., Gu, Q., Zhang, C., Bonifas, J. M., Lam, C.-W., Hynes, M., Goddard, A. et al. (1998). Activating Smoothened mutations in sporadic basal-cell carcinoma. *Nature* **391**, 90-92. doi:10.1038/34201

Yoshiba, S., Shiratori, H., Kuo, I. Y., Kawasumi, A., Shinohara, K., Nonaka, S., Asai, Y., Sasaki, G., Belo, J. A., Sasaki, H. et al. (2012). Cilia at the node of mouse embryos sense fluid flow for left-right determination via Pkd2. *Science* **338**, 226-231. doi:10.1126/science.1222538

Yu, J. K. and Holland, L. Z. (2009). Amphioxus whole-mount in situ hybridization. *Cold Spring Harb. Protoc.* **2009**, pdb-prot5286. doi:10.1101/pdb.prot5286

Yu, X., Ng, C. P., Habacher, H. and Roy, S. (2008). Foxj1 transcription factors are master regulators of the motile ciliogenic program. *Nat. Genet.* **40**, 1445-1453. doi:10.1038/ng.263

Zhang, X. M., Ramalho-santos, M. and Mcmahon, A. P. (2001). Smoothened mutants reveal redundant roles for Shh and Ihh signaling including regulation of L/R asymmetry by the mouse node. *Cell* **105**, 781-792. doi:10.1016/S0092-8674(01)00385-3

Supplementary Tables

Table S1. Primers used for amplifying gene fragments or plasmid construction

Genes/Plasmids	Primer Sequence (5′→3′)	Amplicon sizes (bp)	Enzyme site
Hh	Forward: GAATTTAGCCGTTAATAGGGAG Reverse: GCGAGTAATCCGTCCGTTGA	454	*Bsr*G I
Kif3a	Forward: GTGACAAGAAGGAGCGTGACT Reverse: TCTTACCATTGTATCCCTCCAG	273	*Age* I
Foxj1 TALEN1	Forward 1: GCCACCACTCCAAACCAAAGG Reverse 1: GCAGATCAGGGTTGCGTAGGA	505	*Aji* I
Foxj1 TALEN2	Forward 2: GCCACCACTCCAAACCAAAGG Reverse 2: CTGCCAGCTGGGTTCGGCCA	610	*Bsi*W I
Hh-pXT7	Forward: AATTCGAATTTAGCCGTTAATAGGGAG		*Eco*R I
	Reverse: CTAGTACACACAGCCGAGTAGACACTT		*Spe* I
Smo-pXT7	Forward: GGTACCTTTCCACCATGTTGAGGAGCG		*Kpn* I
	Reverse: CTAGTGGTTCTTCACAGTACTCTGTATC		*Spe* I
Hh-myc-pXT7	Forward1: TTGGCAGATCGGTACCGAATTCATGGCGGGGGT ACTAGCGCG Reverse1: TGAATCCGTCGCCGTTGGGTGT Forward2: ACCCAACGGCGACGGATTCAAAAGAGCTAGCTA CCATGGAGC Reverse2: GATCCTAGTCAGTCACTAGTCTACTCAAGAGGCC TTGAGTTC		
caSmo-myc-pXT7	Forward: ATACGTATGTCACTTATCATAAAGAGCTAGCTAC CATGGAGC Reverse: GATCCTAGTCAGTCACTAGTCTACTCAAGAGGCC TTGAGTTC		

Supplementary Figures

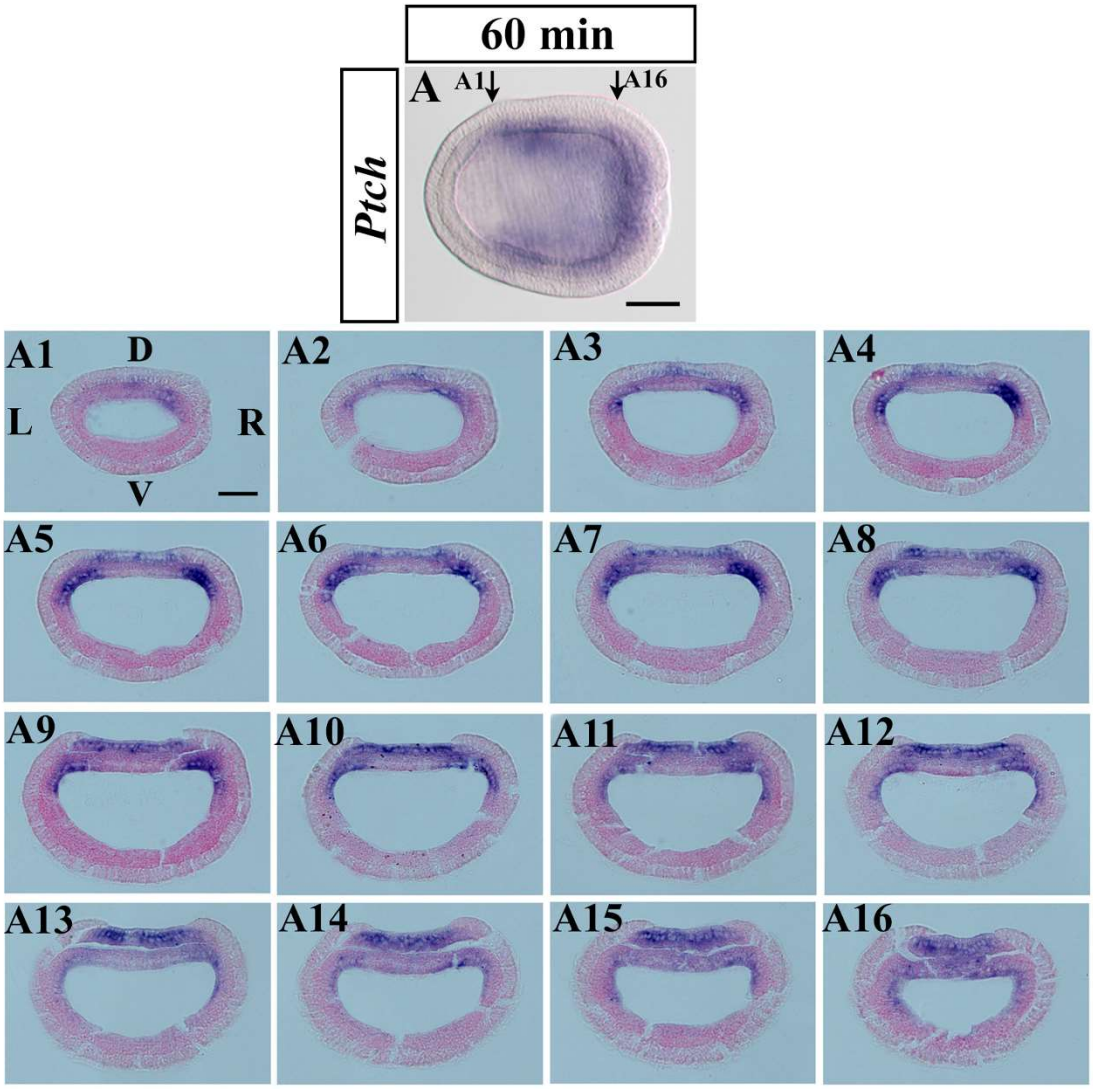

Figure S1. Asymmetric *Ptch* expression in the paraxial mesoderm of amphioxus embryo. (A) The expression of *Ptch* in WT embryo at stage 60 minutes after G5, showing weak asymmetric signal in the anterior paraxial mesoderm when observed from the dorsal side. (A1-A16) Serial transverse sections of the embryo in panel A, between the two arrows. Scale bar in A or A1 is 50 μm.

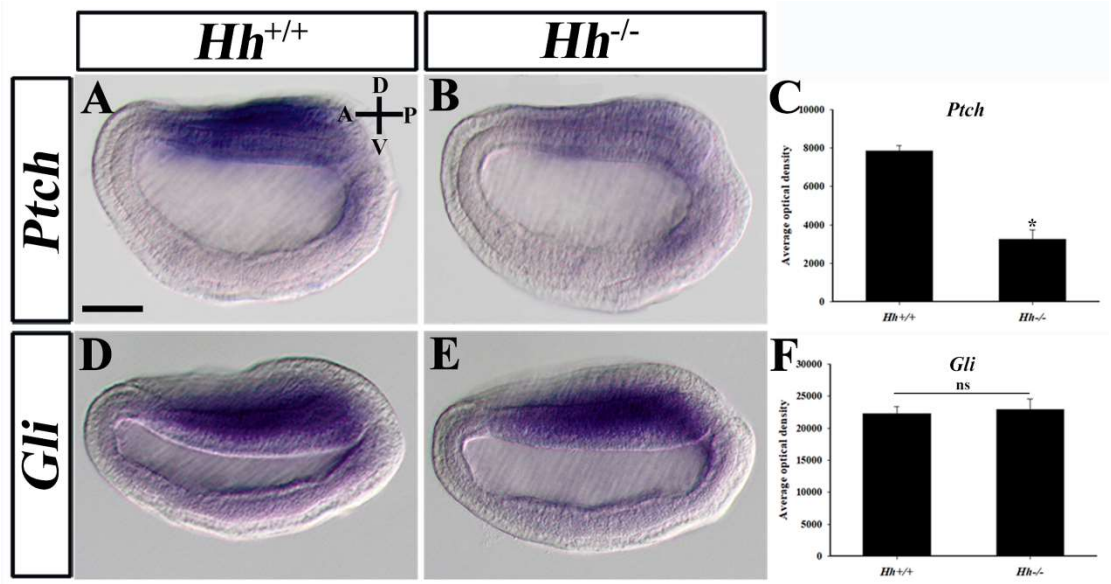

Figure S2. The expression of *Ptch* and *Gli* in *Hh* knockout embryos. (A-C) The expression of *Ptch* was decreased in *Hh* knockout embryos ($P<0.05$, n=4). Scale bar is 50 μm. (D-F) The expression of *Gli* was not significantly different between WT ($Hh^{+/+}$) and *Hh* knockout embryos ($P>0.05$, n=4). * represents statistical significance, ns: not significant.

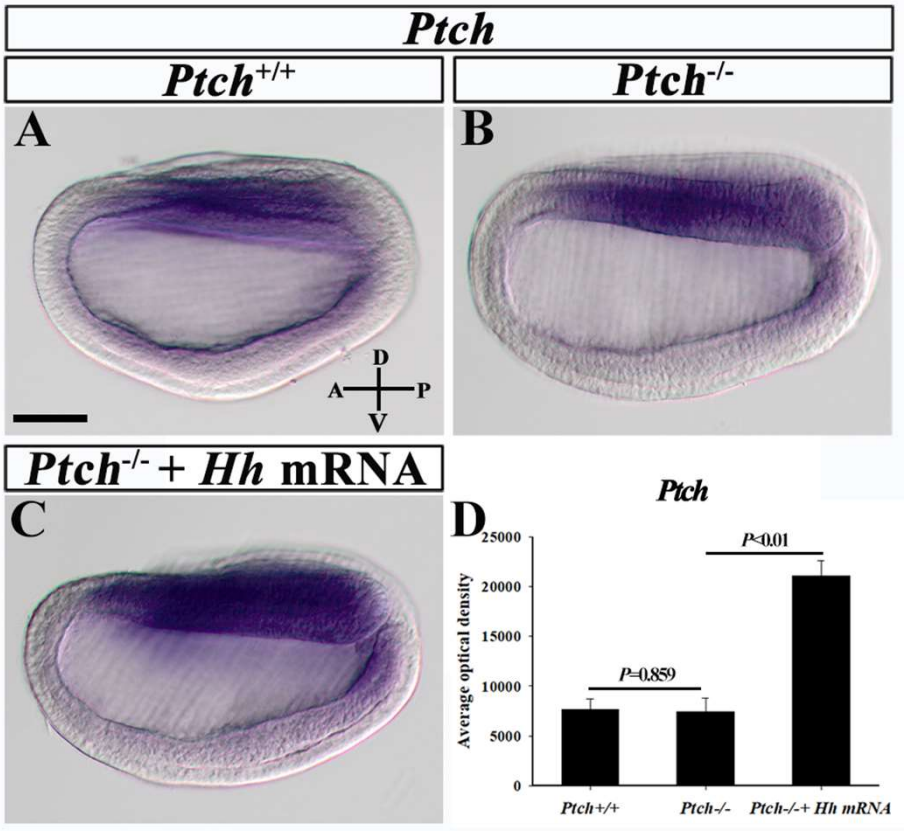

Figure S3. The expression of *Ptch* does not increase in *Ptch* knockout embryos. (A and B) The expression of *Ptch* in WT or *Ptch* knockout embryos. (C) The expression of *Ptch* was increased in *Ptch* knockout embryos injected with *Hh* mRNA. Left-lateral view with anterior to the left. The scale bar in A is 50 μm, and applies to B and C. (D) The optical density of *Ptch* expression in WT, *Ptch* knockout embryos and *Ptch* knockout embryos injected with *Hh* mRNA. The expression of *Ptch* was not significantly different between WT and *Ptch* knockout embryos ($P>0.05$, n=4), but was remarkably up-regulated in *Ptch* knockout embryos injected with *Hh* mRNA ($P<0.05$, n=4).

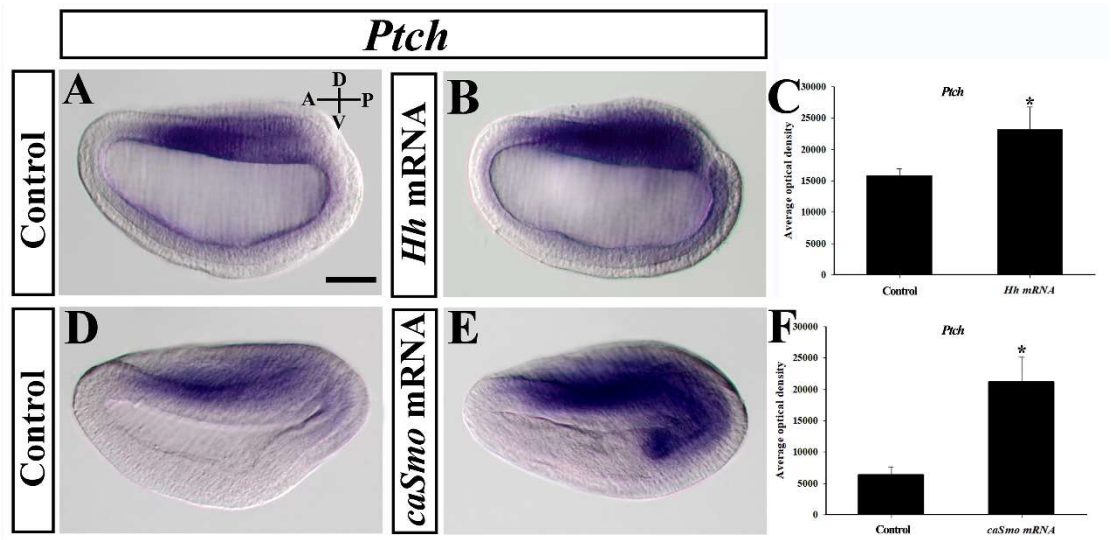

Figure S4. *Ptch* expression is increased in *Hh* or *caSmo* mRNA-injected embryos. Left-lateral view with anterior to the left. The scale bar (50 μm) in A applies to all panels. (A, B) The expression of *Ptch* in control and *Hh* mRNA-injected embryos. (C) The optical density of *Ptch* expression in control and *Hh* mRNA-injected embryos (n=6, $P<0.05$). (D, E) The expression of *Ptch* in control and *caSmo* mRNA-injected embryos. (F) The optical density of *Ptch* expression in control and *caSmo* mRNA-injected embryos (n=6, $P<0.05$). * represents statistical significance.

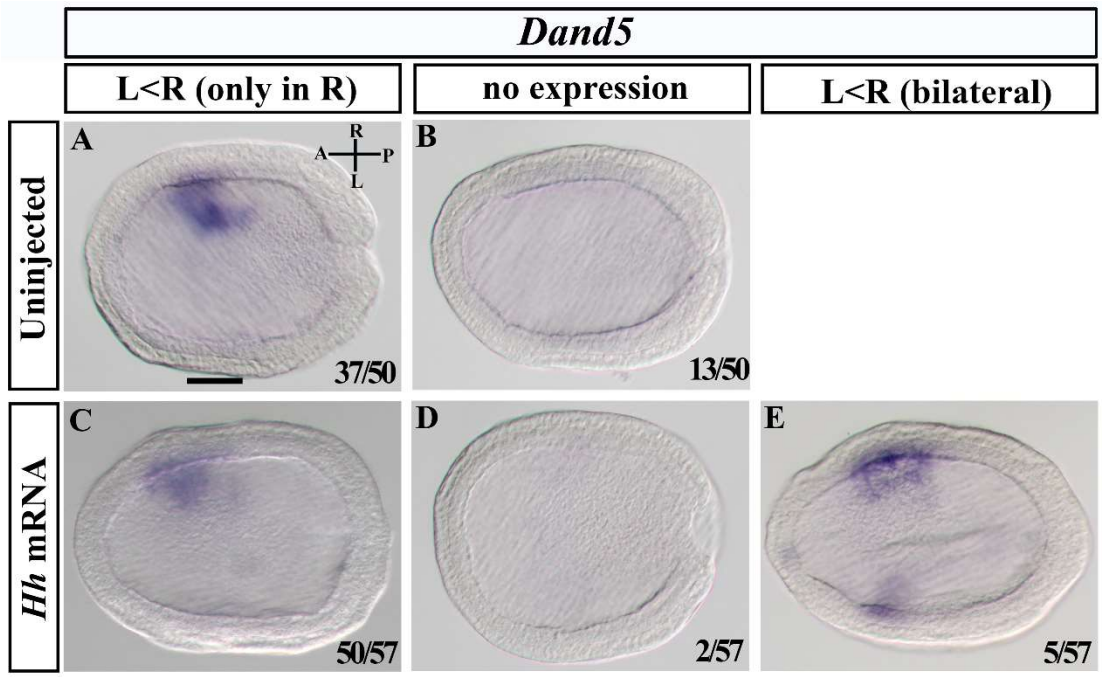

Figure S5. *Hh* mRNA injection rescues *Dand5* expression (R>L) in $Hh^{-/-}$ embryos, but could not induce L=R or L>R *Dand5* expression. Dorsal view with anterior to the left. (A, B) Expression patterns of *Dand5* in offspring of $Hh^{+/-}$ heterozygotes. (A) Right-side specific *Dand5* expression in WT/$Hh^{+/-}$ embryos. (B) Loss of *Dand5* expression in $Hh^{-/-}$ embryos. (C-E) Expression patterns of *Dand5* in *Hh* mRNA injected offspring of $Hh^{+/-}$ heterozygotes. Most of the injected embryos show right-side specific *Dand5* expression (C), and a few of them show no (D) or L<R (bilateral) *Dand5* expression (E). Numbers in the bottom right corner of a panel show the number of times the phenotype was observed in the total number of embryos examined. Scale bar (50 μm) in A applies to all panels.

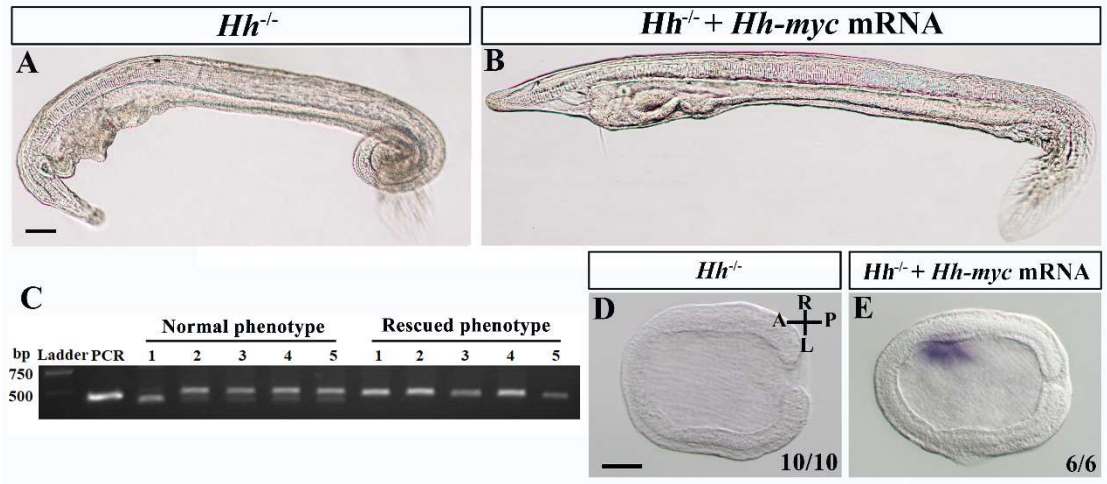

Figure S6. *Hh-myc* mRNA injection rescues the L-R morphological defects and *Dand5* expression in *Hh*$^{-/-}$ amphioxus. (A) The phenotype of *Hh*$^{-/-}$ larvae, showing a curled head, no mouth, ventralized gill slits and twisted tail. (B) Morphological restoration of *Hh*$^{-/-}$ larvae after injection of *Hh-myc* mRNA. (C) Genotyping of *Hh-myc* mRNA-injected offspring of *Hh*$^{+/-}$ heterozygotes. The normal phenotype refers to morphology of WT larvae, and the rescued phenotype refers to morphology as shown in panel B. (D) The expression of *Dand5* in *Hh*$^{-/-}$ embryos. (E) The expression of *Dand5* in *Hh*$^{-/-}$ embryos injected with *Hh-myc* mRNA. The injection rescued asymmetric *Dand5* expression in *Hh*$^{-/-}$ embryos. Scale bar in A or D represents 50 μm.

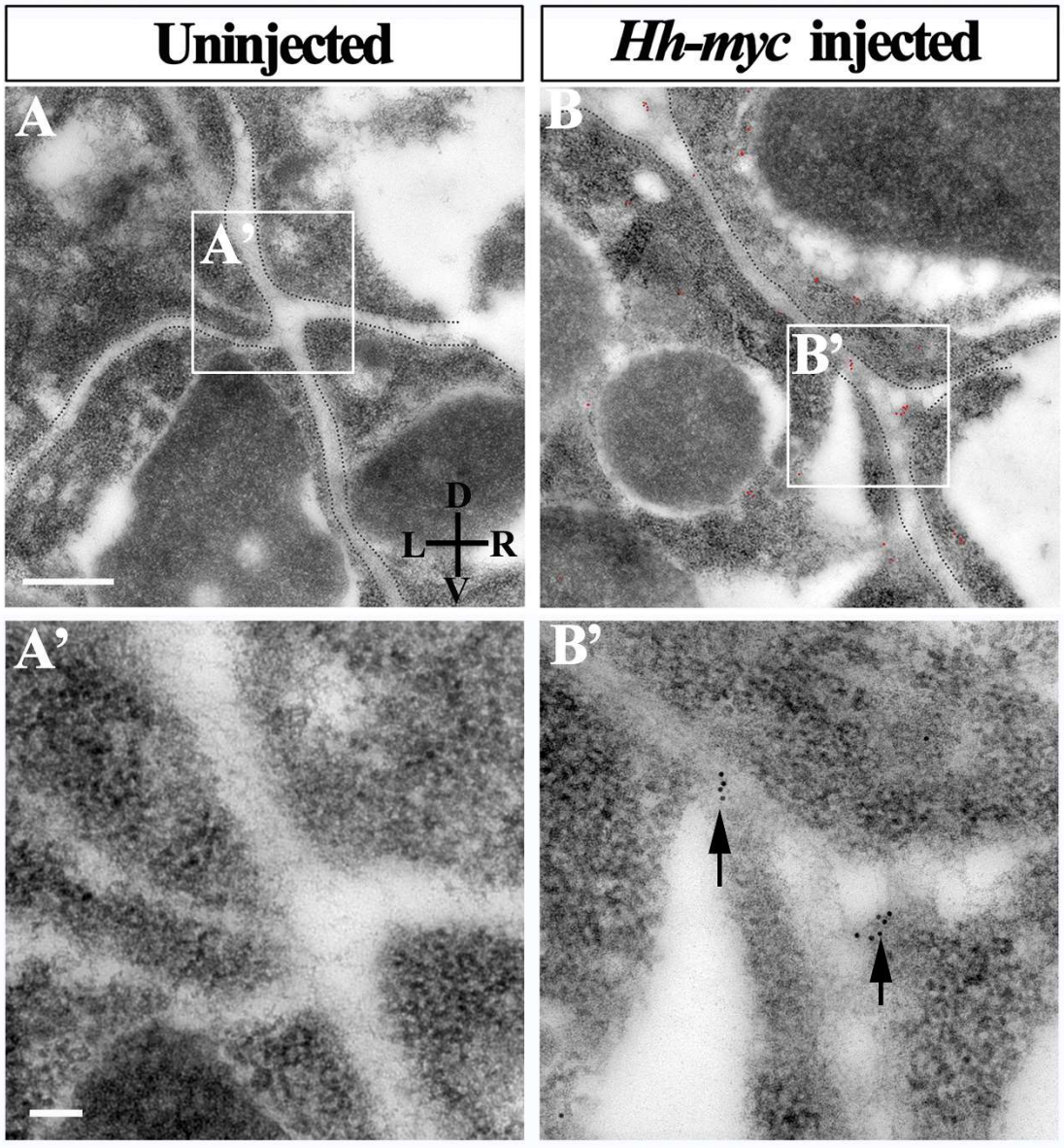

Figure S7. Immuno-EM localization of Hh-Myc fusion protein in the right side of paraxial mesoderm of *Hh-myc* mRNA-injected embryo. (A, B) Immuno-EM image of the right side of uninjected and the *Hh-myc* mRNA-injected embryos at early neurula stage. The dotted lines indicate the boundary of each cell, and the red dots represent Hh-Myc protein labelled with gold particles. R: Right; L: Left. D: Dorsal; V: Ventral. Scale bar = 500 nm. (A') Local zoom of the region in the box in panel A. Hh-Myc fusion protein is not observed in uninjected embryos. (B') Local zoom of the region in the box in panel B. Arrows point to Hh-Myc fusion protein localized to the extracellular of paraxial mesoderm. Scale bar in A' is 100 nm.

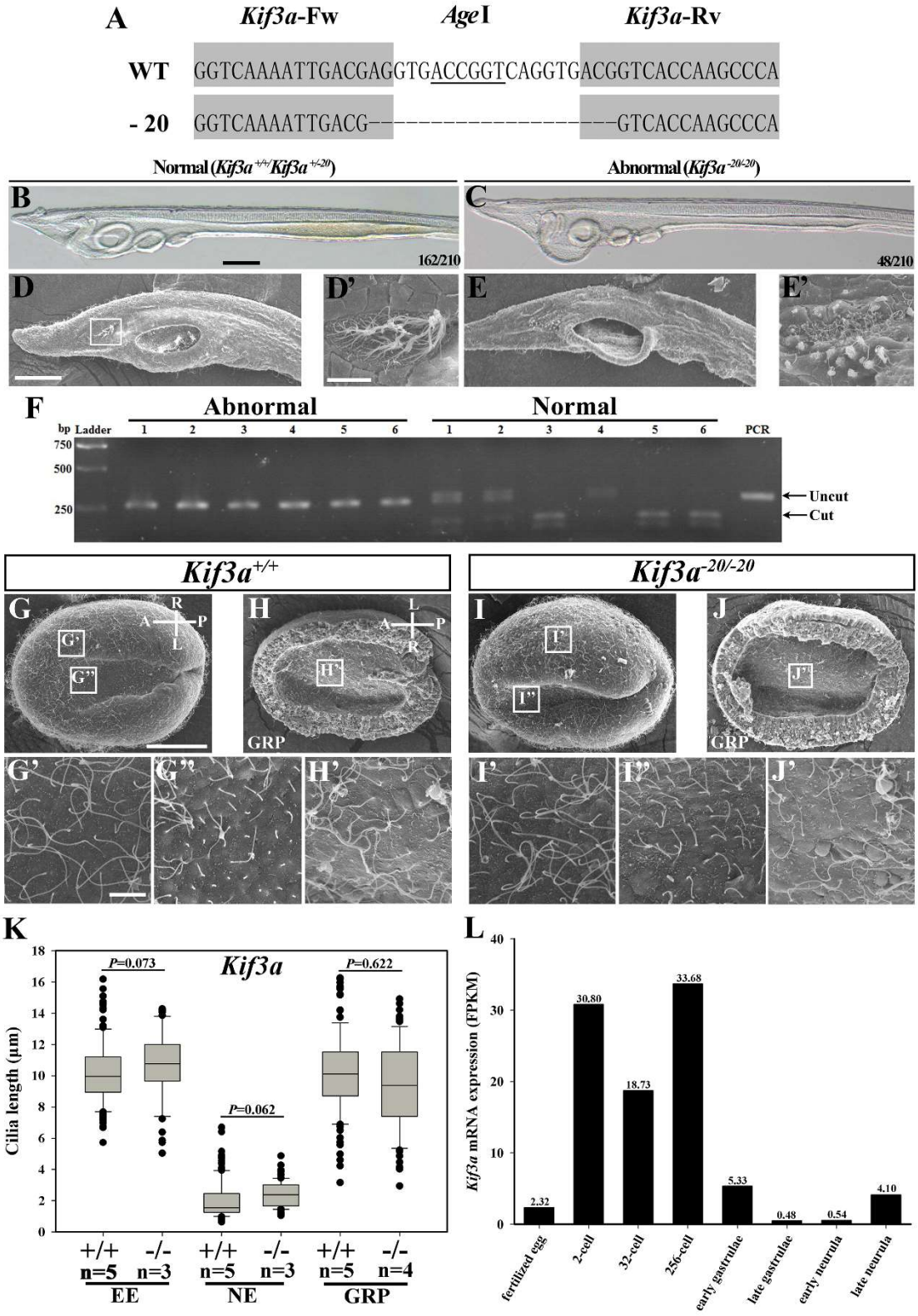

Figure S8. The ciliogenesis in *Kif3a* knockout amphioxus mutant. (A) The binding sites for *Kif3a* TALEN pairs (greyed) and the mutation type used in the study. (B and D) Left lateral view of WT/*Kif3a*$^{+/-}$ larvae. Scale bar in B or D is 50 μm. (D') Local

zoom of the preoral pit in the box in D, showing abundant cilia in this region. Scale bar in D' is 10 μm. (C and E) Left lateral view of *Kif3a*$^{-/-}$ larvae. The larva developed an enlarged mouth. (E') Local zoom of the preoral pit in the box in D, showing sparse cilia in this region. Numbers in the bottom right corner of panel B and C show the number of times the phenotype was observed in the total number of embryos examined. (F) Genotype analysis of abnormal and normal phenotype larvae using PCR assay. All six larvae of abnormal phenotype are *Kif3a*$^{-/-}$ mutants, and all six larvae of normal phenotype are WT or *Kif3a*$^{+/-}$ mutants. (G-J) SEM analysis of epithelial ectodermal (EE), neural ectodermal (NE) and gastrocoel roof plate (GRP) cilia of WT and *Kif3a*$^{-/-}$ early neurula. Anterior to the left. Scale bar (50 μm) in G applies to G-J and that (5 μm) in G' applies to G'-J'. (K) Quantification of cilia length in *Kif3a*$^{+/+}$ and *Kif3a*$^{-/-}$ embryos. The cilia length on EE, NE or GRP cells was not significant different between WT and *Kif3a*$^{-/-}$ embryos. n represents number of embryos analyzed, 20-40 cilia from each region were counted for every embryo. (L) The expression pattern of *Kif3a* during embryonic development according to transcriptome dataset.

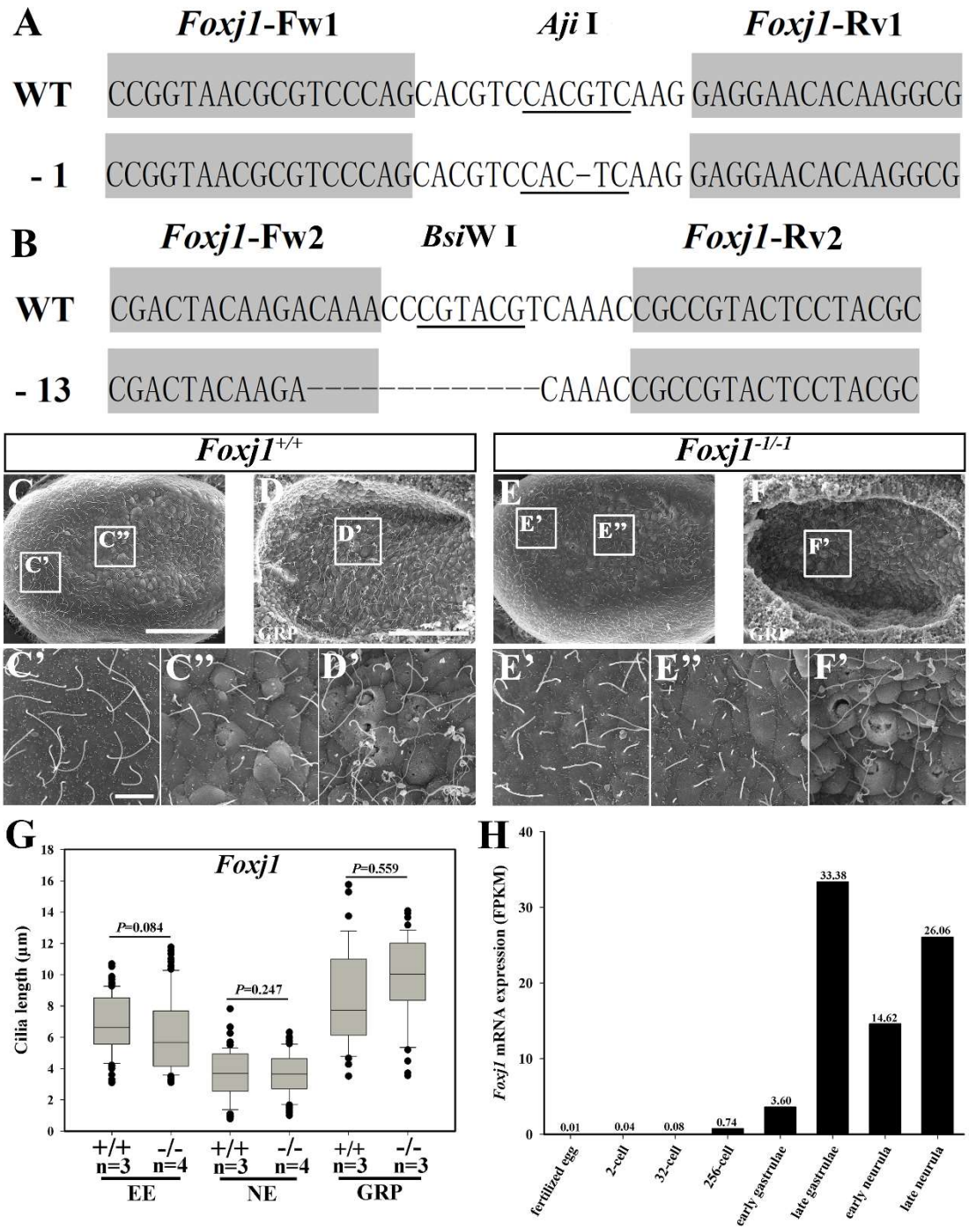

Figure S9. The ciliogenesis in *Foxj1* mutants. (A, B) The binding sites for two *FoxJ1* TALEN pairs (greyed) and the mutation types used in the study. (C-F) SEM analysis of epithelial ectodermal (EE), neural ectodermal (NE) and gastrocoel roof plate (GRP) cilia of *Foxj1*$^{+/+}$ and *Foxj1*$^{-1/-1}$ embryos. Anterior to the left. Scale bar in C or D is 50 μm. Scale bar in C' is 5 μm. (G) Quantification of cilia length in *Foxj1*$^{+/+}$ and *Foxj1*$^{-1/-1}$ embryos. The cilia length on EE, NE or GRP cells was not significant different between WT and *FoxJ*$^{-1/-1}$ embryos. n represents number of embryos analyzed, 20-40 cilia from each region were counted for every embryo. (H) The expression pattern of *Foxj1* during embryonic development according to transcriptome dataset.

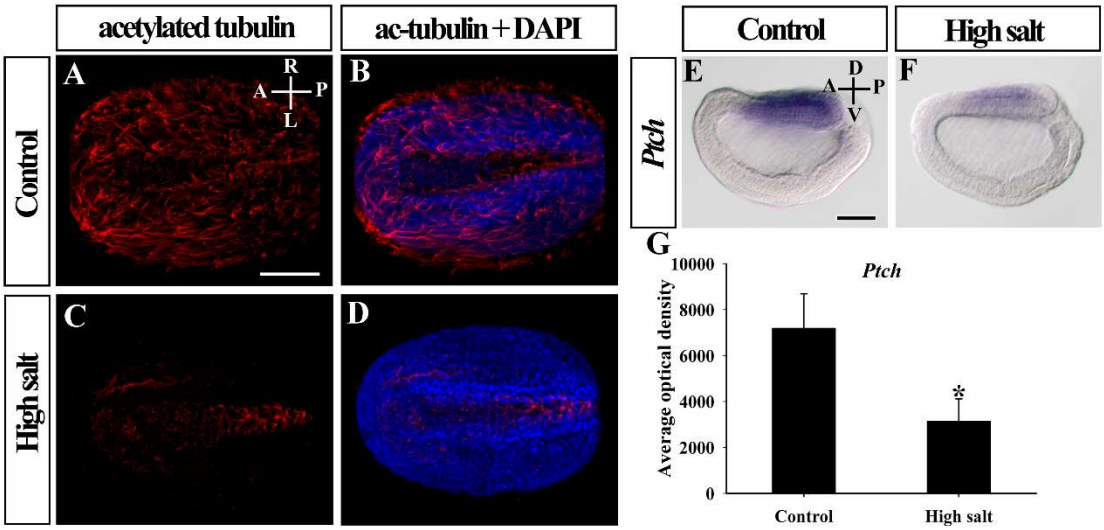

Figure S10. Removal of cilia results in down-regulation of Hh signaling activity in amphioxus. (A-D) Cilia in control and high salt (HS) treatment embryos, displaced by immunofluorescence with the cilia-specific acetylated tubulin antibody (red). Images in panels A-D were taken from the dorsal side with anterior to the left. Cell nucleuses are labelled with DAPI (blue). Most cilia in epidermal ectoderm and neurectoderm were removed by HS treatment. Scale bar is 50 μm. (E, F) The expression of *Ptch* in control and HS-treated embryos. Left lateral view with anterior to the left. Scale bar in E is 50 μm. (G) The average optical density in control and HS-treated embryos. It was significantly decreased in HS-treated embryos ($P < 0.01$, n=6). * represents statistical significance.

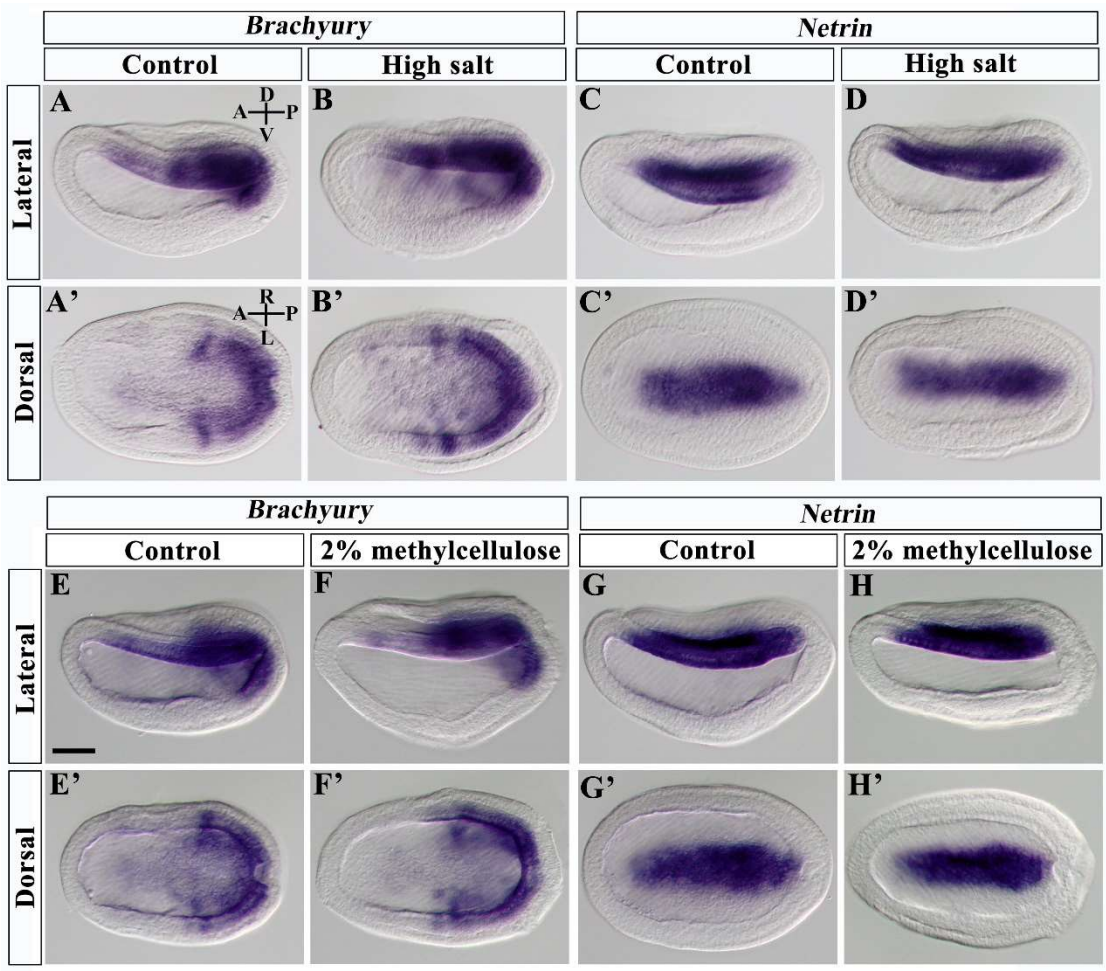

Figure S11. The expression pattern of midline structure marker genes in high salt treated and methylcellulose treated embryos at early neurula stage. (A-D) The expression of *Brachyury* and *Netrin* in control or high salt treated embryos. There was no obvious difference between control and the treated embryos. (E-H) The expression of *Brachyury* and *Netrin* in control or methylcellulose treated embryos. There was no obvious difference between control and treated embryos. The scale bar (50 μm) in E applies to all panels.

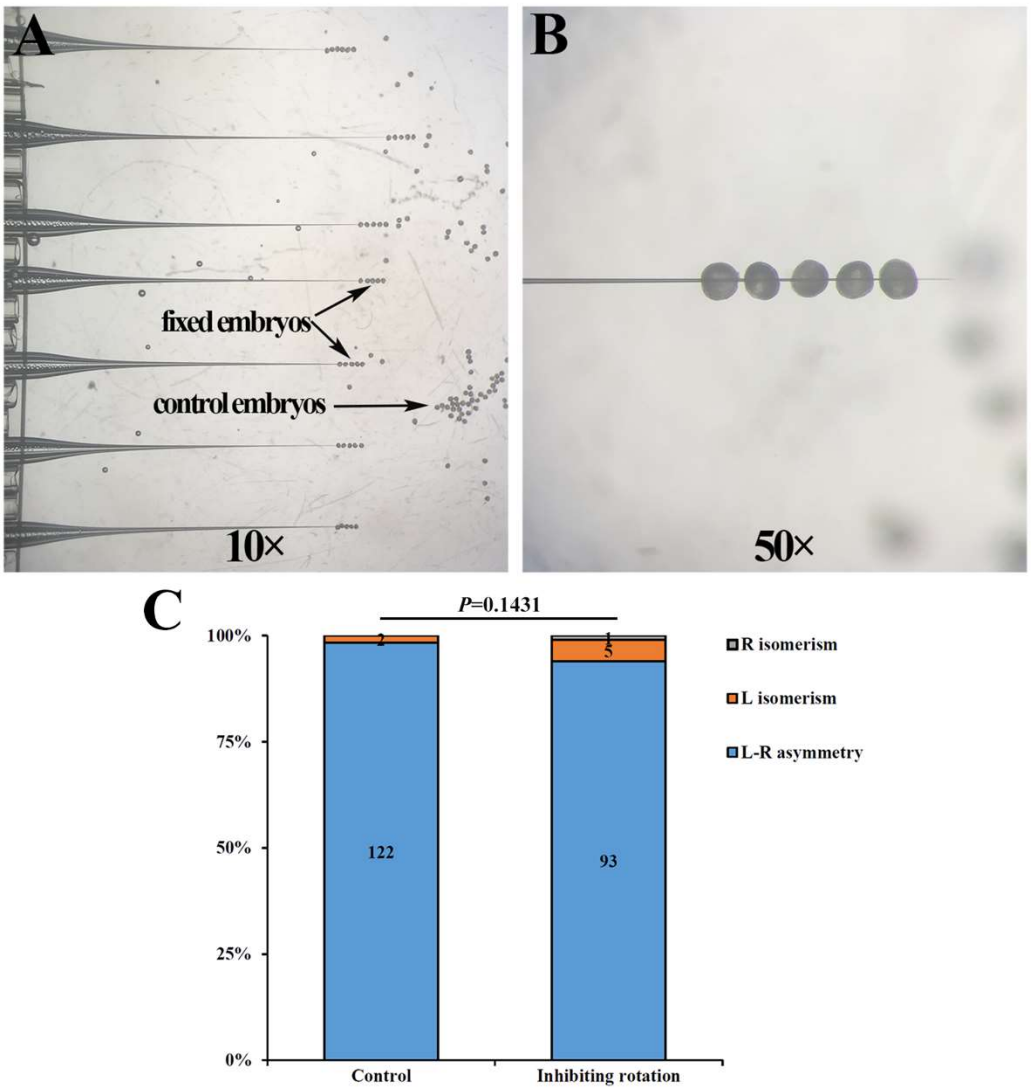

Figure S12. Embryo rotation is not essential for L-R asymmetry development in amphioxus. (A, B) 10× and 50× optical magnification of embryos, respectively. The embryos were fixed by threading them on very fine glass needles at G4 stage. (C) Percentages of embryos showing each type of phenotypes. The numbers in the column represent the number of each phenotype observed.

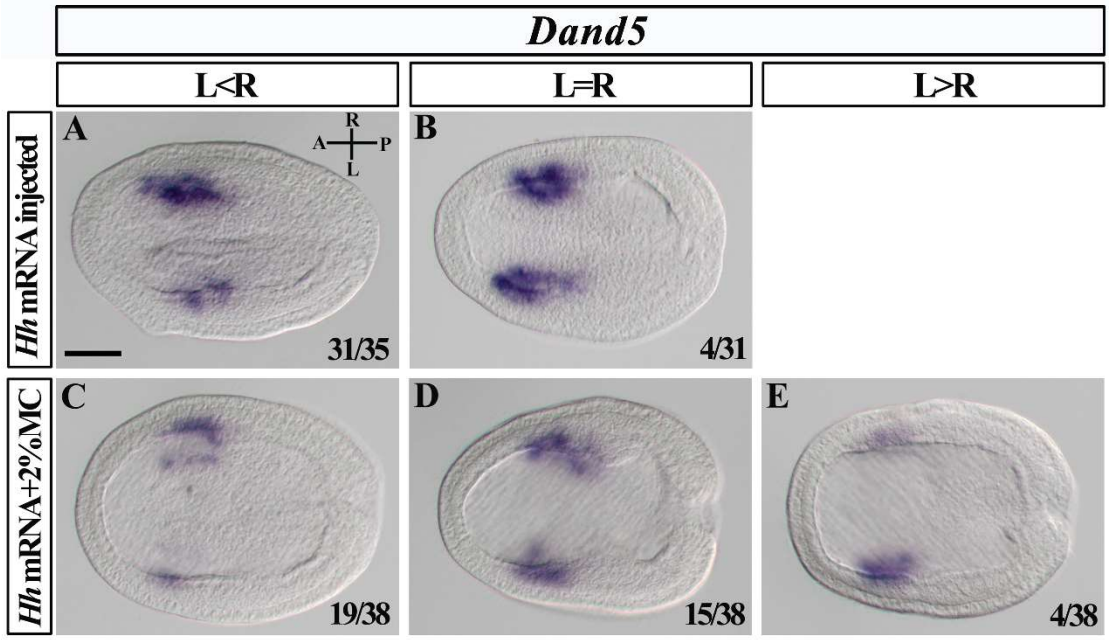

Figure S13. Inhibiting cilia movement increases the frequency of bilateral (L=R) *Dand5* expression in *Hh* mRNA injected wildtype embryos. Images in panels A-E were taken from the dorsal view with anterior to the left. (A, B) *Dand5* expression patterns in *Hh* mRNA injected embryos. (C-E) *Dand5* expression patterns in *Hh* mRNA injected embryos cultured in 2% methylcellulose. Numbers in the bottom right corner of a panel show the number of times the phenotype was observed in the total number of embryos examined. Scale bar (50 μm) in A applies to all panels.

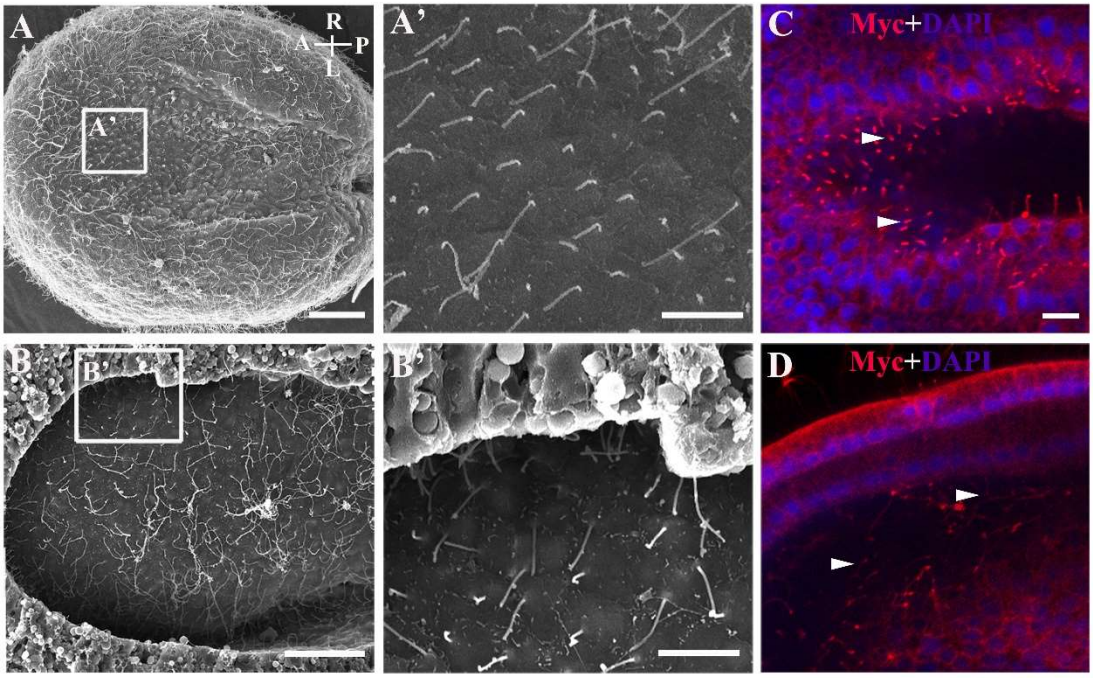

Figure S14. Hh-receiving cells own motile cilia and Smo localizes to these cilia. (A and A') SEM analysis of cilia on neural ectodermal cells of wildtype early neurula embryo. Dorsal view with anterior to the left. A' is a local zoom of the region in the box in panel A. Scale bars in A or A' is 20 or 5 μm, respectively. (B and B') SEM analysis of cilia on paraxial mesodermal cells of wildtype early neurula embryo. Ventral view with anterior to the left. B' is a local zoom of the region in the box in panel B. Scale bar in B or B' is 20 or 5 μm, respectively. (C and D) Localization of caSmo fusion protein in the cilia of neural ectodermal cells and paraxial mesodermal cells. Image C was dorsal view focusing on the neuroderm. Image D was dorsal view focusing on the paraxial mesoderm. caSmo fusion protein was labelled with the Myc antibody (red) and cell nucleuses were labelled with DAPI (blue). The arrowheads point to the cilia location of caSmo fusion protein. Scale bar in C is 10 μm.

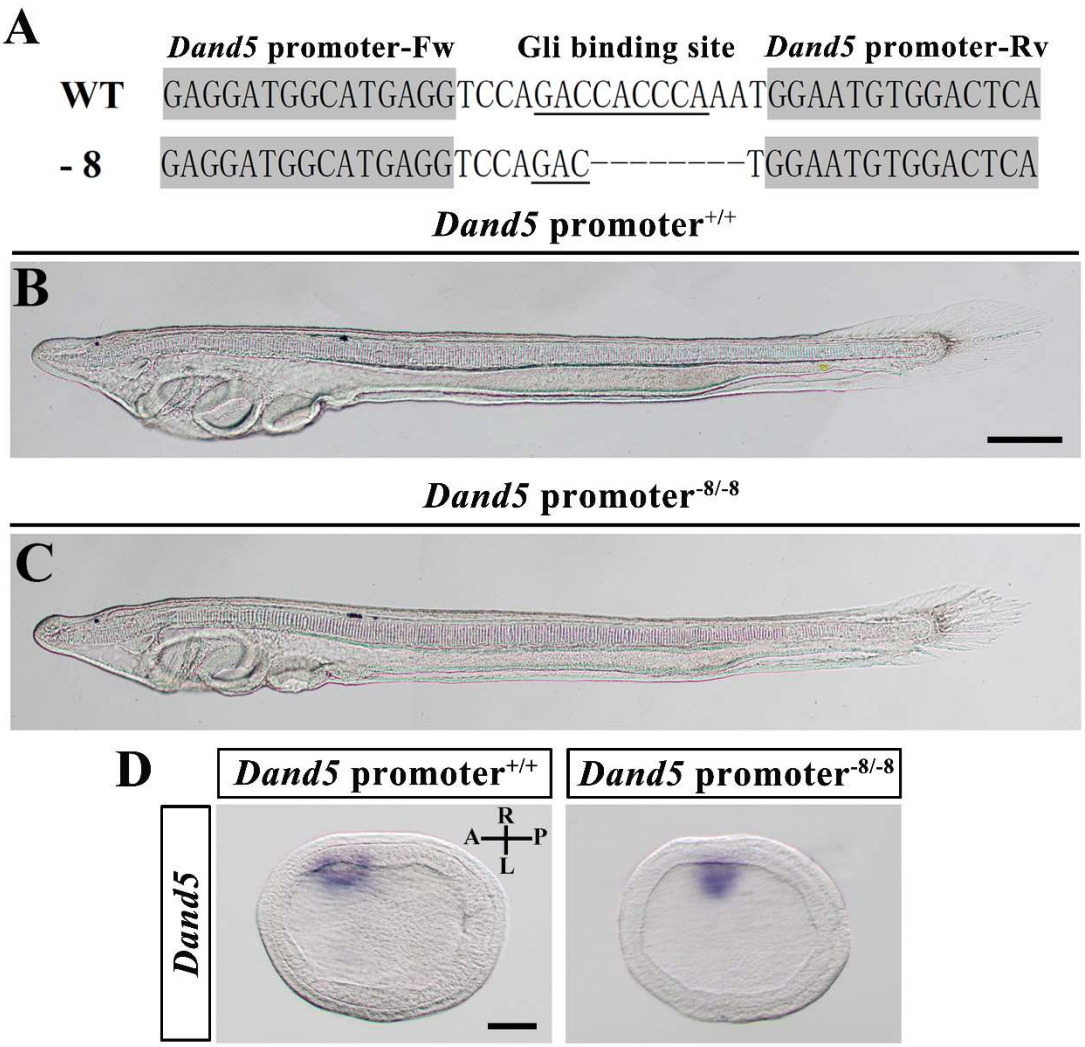

Figure S15. TALEN pairs targeting Gli binding site in *Dand5* promoter and phenotype analysis of the F2 embryos. (A) The binding site for the TALEN pair (greyed) and the mutation type used in the study. The Gli binding site in the spacer was underlined. (B and C) Left lateral view of the *Dand5* promoter$^{+/+}$ larva and *Dand5* promoter$^{-8/-8}$ larva. No obvious morphological difference was observed between them. (D) Expression patterns of *Dand5* in *Dand5* promoter$^{+/+}$ embryos and *Dand5* promoter$^{-8/-8}$ embryos. No obvious expression difference was observed between them. Image in D was taken from the dorsal view with anterior to the left. Scale bar in B or D is 50 μm.

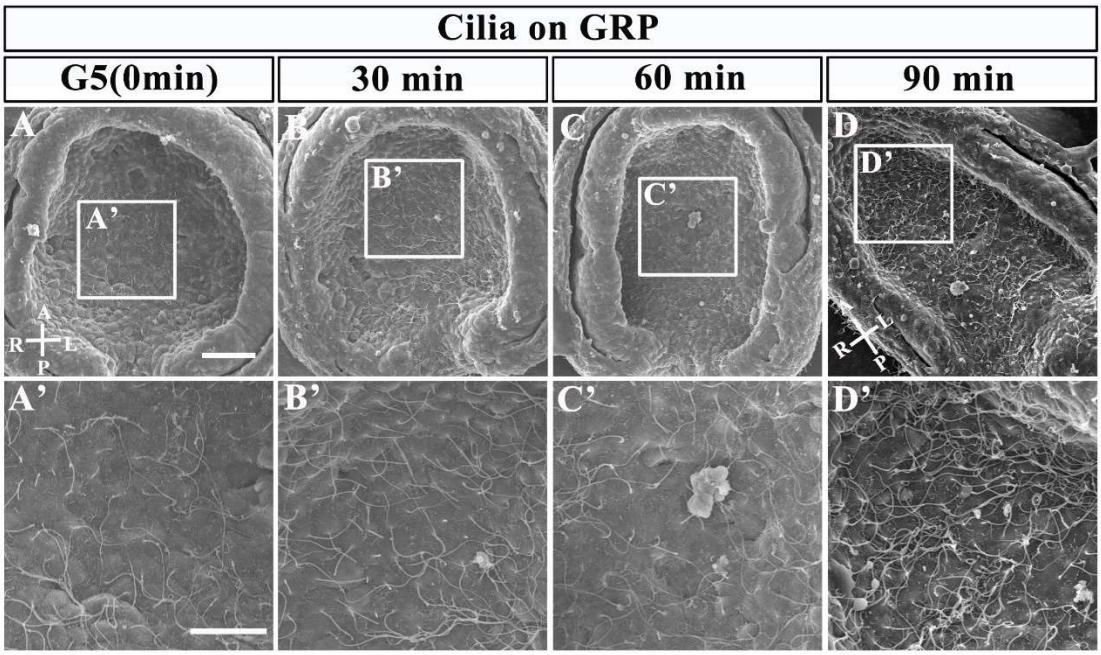

Figure S16. Observation of cilia on gastrocoel roof plate (GRP). Images in panels A-D were taken from the ventral view. 'A' anterior; 'P' posterior; 'L' left side; 'R' right side. (A-D) SEM analysis of cilia on GRP, time at G5 stage was defined as 0 minute, and 3 stages after that were adopted in the analysis. (A'-D') Local zoom of the region in the box in panel A-D, respectively. Scale bar in A or A' is 20 or 10 μm, respectively.

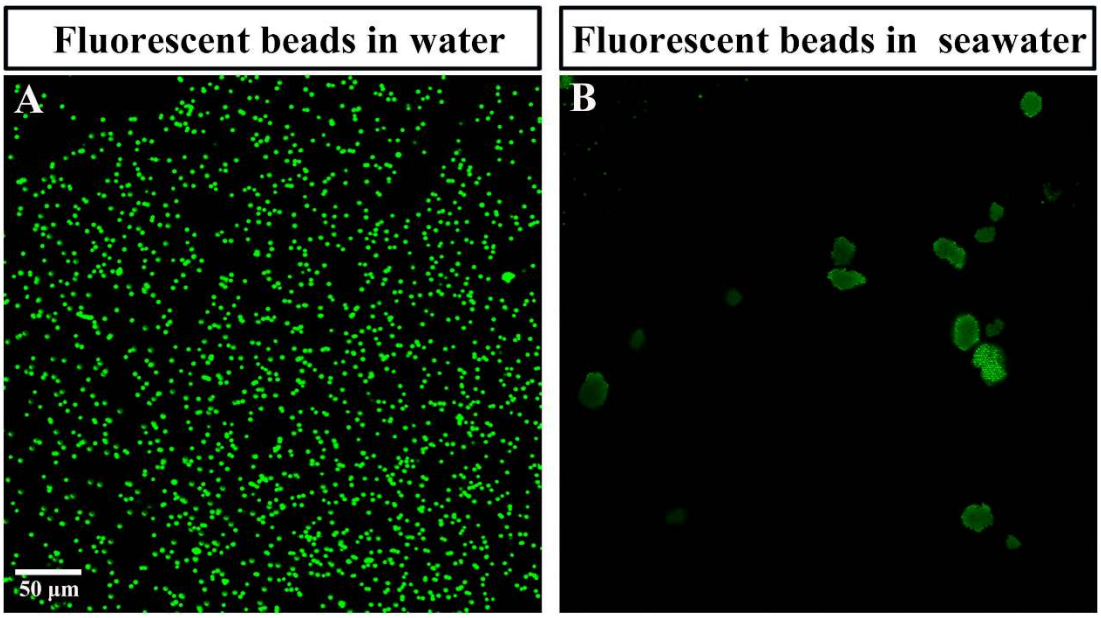

Figure S17. Dispersion of fluorescent beads in water and seawater. (A) Fluorescent beads were well dispersed in water. (B) Fluorescent beads easily gathered into big blocks in seawater.

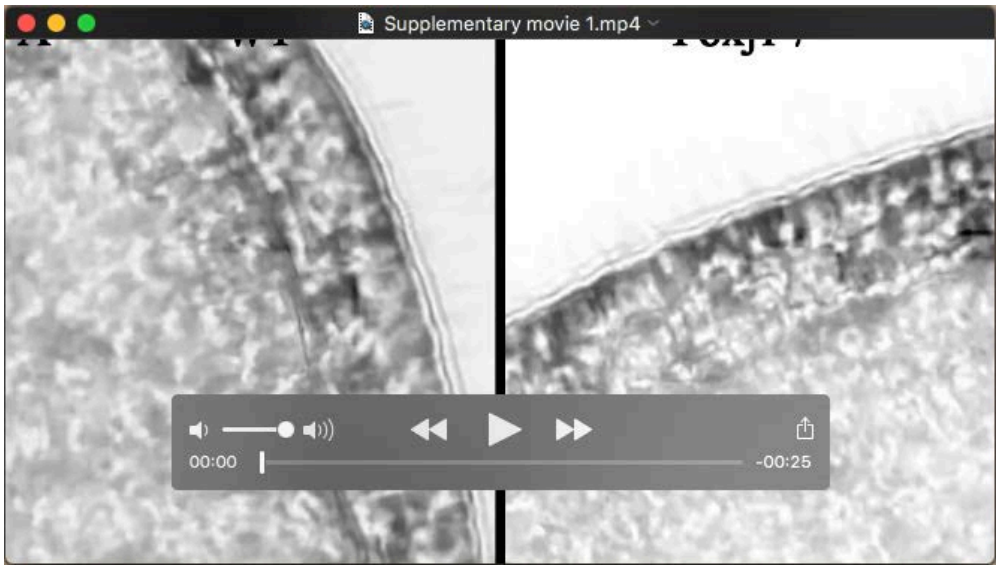

Movie 1. Cilia movement of *Foxj1*$^{-1/-1}$ homozygous mutants are of no apparent defects. Real-time movie of *Foxj1*$^{-1/-1}$ neurula embryo reveals normal cilia movement on the epithelial ectodermal cells, neural ectodermal cells and gastrocoel roof plate cells, compared to that in wildtype embryos. A, B or C in the movie showed ciliary motility in epithelial ectoderm, neural ectoderm or gastrocoel roof plate, respectively.

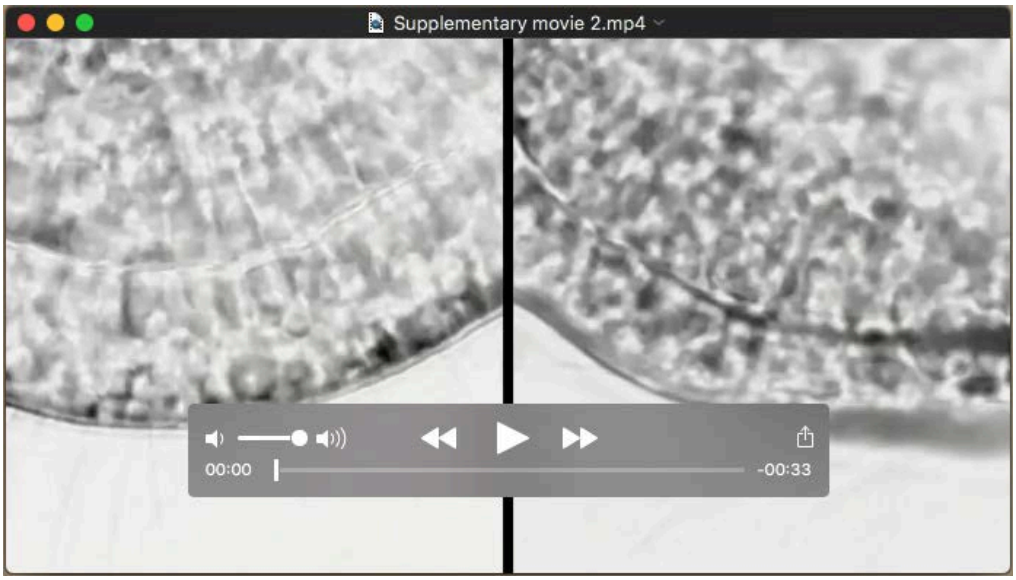

Movie 2. Ciliary motility is inhibited by 2% methylcellulose. Real-time movie of ciliary motility in control and methylcellulose treated embryo. A, B or C in the movie showed ciliary motility in epithelial ectoderm, neural ectoderm or gastrocoel roof plate, respectively. D in the movie showed neurula rotation. Motility of cilia on the epithelial ectodermal cells, neural ectodermal cells or gastrocoel roof plate cells was effectively inhibited by methylcellulose. Furthermore, neurula rotation was completely inhibited by methylcellulose.

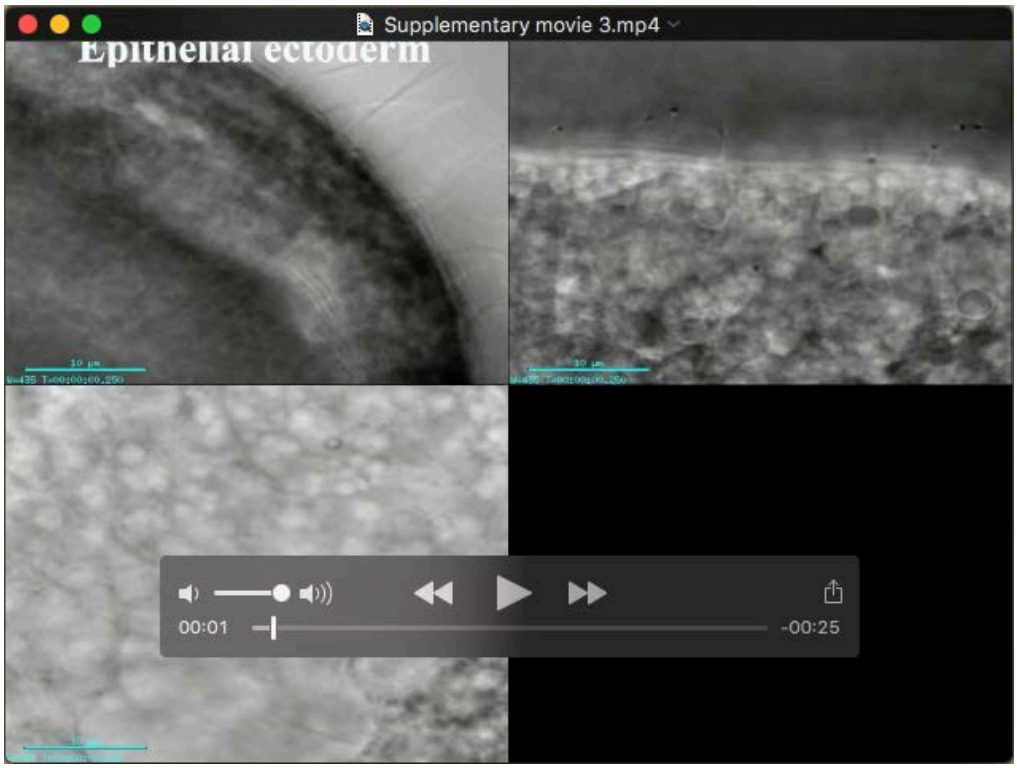

Movie 3. Cilia in early neurula embryos of amphioxus are motile, but do not rotate. Time-lapse movie of dorsal explant of early neurula (ventral view) revealed fast beating of long cilia on left-lateral epithelial ectodermal cells, and very low-frequency of beating of long cilia on gastrocoel roof plate cells, and medium-frequency beating of short cilia on anterior neural ectodermal cells. For better observation, the movie was slowed down to half of its original speed. The bars in the movie are 10 μm.